The Thesis Committee for Michael Slovich III
Certifies that this is the approved version of the following thesis:

Case Studies in Multi-Contact Locomotion

APPROVED BY

SUPERVISING COMMITTEE:

Luis Sentis, Supervisor

Benito Fernandez

Case Studies in Multi-Contact Locomotion

by

Michael Slovich III, B.A.

THESIS

Presented to the Faculty of the Graduate School of

The University of Texas at Austin

in Partial Fulfillment

of the Requirements

for the Degree of

MASTER OF SCIENCE IN ENGINEERING

THE UNIVERSITY OF TEXAS AT AUSTIN

May 2012

To my loving parents and sister

Acknowledgments

There are many people who have made this thesis possible and whom I would like to thank. First and foremost, I would like to thank my advisor, Dr. Luis Sentis, for his support and guidance. I am consistently amazed at his passion for robotics and even more so at the concern he has for his students. I can think of no one who I would have preferred to study under in his stead. I would also like to thank Dr. Benito Fernandez for his help in the development of the material covered in this thesis and for serving as my second reader.

Next, I would like to thank my HCRL labmates. Nick Paine has been a consistent source of advice for me from my first day in the lab. Thank you, I greatly appreciate your help. Ye Zhao has also been a crucial source of advice for me. Thank you for letting me bounce ideas off of you and for your patience while I did so. The rest of the HCRL including Kenan Isik, Kwan Suk Kim, Pius Wong, Dr. Seung Kyu Park, Somudro Gupta, Matt Gonzalez, Sehoon Oh and Ho Jin Kang all deserves special recognition. Thanks to all of you guys - you are more than just labmates to me - you are friends.

Lastly, I would like to thank my parents, Mike and Sue, and my sister, Amanda, for their love and support not just during my time in graduate school but throughout my life. Without you I don't know where I'd be.

Case Studies in Multi-Contact Locomotion

Michael Slovich III, M.S.E
The University of Texas at Austin, 2012

Supervisor: Luis Sentis

The problem of performing complex maneuvers in challenging terrains is crucial to the advancement of legged robots and assistive devices, yet little progress has been made in exploring practical solutions to operate in these environments. In this thesis, we tackle the problem by developing strategies to predict a robot's center of mass (CoM) behavior based on contact constraints, and any arbitrary CoM path for situations in which the system has single or multiple points of contact through which external reaction forces may be applied. Our method consists of first leveraging previous work on multi-contact dynamics to derive reaction force behavior from internal tension force profiles and kinematic CoM trajectories. We then study the nonlinear dynamics of single contact phases along arbitrary paths and employ numerical integration to derive state-space approximations of CoM behavior. We use this theoretical framework to synthesize complex maneuvers in various terrains by means of a motion planner in which we determine step transition sequences for continuous motions involving contact profiles which vary with time.

Furthermore, we validate our strategy through several comparative case studies, examining the motion of a human subject performing a difficult maneuver in an aggressive terrain. We then seed our motion planning algorithm with a limited set of parameters chosen to match those of a human subject and predict CoM behavior for the same motion pattern. These case studies show that the estimated CoM behaviors generated from our planning algorithm closely resemble the behavior of the human subject and therefore validate our methods.

Table of Contents

List of Figures

Chapter 1

Introduction

A broad goal of the Human Centered Robotics Laboratory (HCRL) at the University of Texas at Austin (UT-Austin) is to understand the physical capabilities and physiology of human movement for use in the design of robots and assitive devices with similar abilities. This study and design process has a basis in the planning and sequencing of contact transitions during complex multi-contact motions in varied terrains. In this thesis, we will focus on several case studies related to these topics and employ planning algorithms developed in collaboration with research advisor, Dr. Luis Sentis. These algorithms have the ability to plan moderately complex motions such as walking over obstacles up to very complicated, extreme maneuvers such as those executed during the sports of parkour and freerunning where athletes traverse near vertical surfaces to navigate through challenging urban environments.

1.1 State of the art in locomotion planning

Let us first look at the current state of the art in locomotion planning. We can classify dynamic walking techniques into various categories: (1) trajectory-based techniques, (2) limit cycle-based techniques, (3) prediction of

contact, and (4) hybrids of the previous three.

Trajectory-based techniques are techniques that track a time-based joint or task space trajectory according to some locomotion model such as the *Zero Moment Point* (ZMP). State of the art trajectory-based techniques include generalized multi-contact locomotion behaviors developed in [6], and more recently, a time delay extension to the ZMP method for locomotion in moderately uneven terrain developed in [9].

Prediction of contact placement are techniques that use dynamics to estimate suitable contact transitions to produce locomotion or regain balance. In [15], simple dynamic models are used to predict the placement of subsequent contacts to achieve desire gait patterns. Finding feasible center of mass (CoM) static placements given frictional constraints was tackled in [2, 4]. In [14], *stable locomotion*, the wide sense of not falling down is studied by providing velocity based stability margins. This work is used to regain stability when the robot is pushed out, and led to the concept of *Capture Point*.

Limit cycle based techniques were pioneered in [11] through the field of *passive dynamic walking*. In [5] the authors study orbital stability, and the effect of feedback control to achieve asymptotic stability. Optimization of open-loop stability is investigated in [12]. In [16], the authors analyze the energetic cost of bipedal walking and running as well as the role of leg sequencing. In [23], the authors developed a dynamic walker using artificial muscles and principles of stability from passive walkers. In [24], a methodology for the analysis of state-space behavior and feedback control are presented for

various physical robots. *Step recovery* in response to perturbations is studied in [22] supported by a linear bipedal model in combination with an orbital energy controller. In [17], the selection of gait patterns based on studying the interplay between robustness against perturbations and leg compliance is investigated.

Hybrid methods include [26], where the stability of passive walkers is studied and a controller obeying the rule, "in order to prevent falling backward the next step, the swing leg shouldn't be too far in front," is suggested. Stochastic models of stability and its application for walking on moderately rough unmodeled terrain are studied in [3]. The design of non-periodic locomotion for uneven terrain is investigated in [10]. In [21], the authors explore the design of passivity-based controllers to achieve walking on different ground slopes. Optimization-based techniques for locomotion in rough terrains are presented in [28]. Locomotion in very rough terrain is presented in [7], where the authors exploit optimization and static models as a means to plan locomotion. More recently, the authors of [1] have proposed a very efficient planner that can generate a discrete sequence of multi-contact stances using static criteria.

1.2 State of the art in multi-contact modeling

The work discussed in this thesis connects with the role of internal forces in terms of acceleration capabilities, thus we will briefly review the state of the art in this area. Initial research on modeling multi-contact be-

haviors and the associated internal forces acting between manipulators can be found in [13]. Using a closed-chain mechanism called the *virtual linkage model*, decoupled object behavior and accurate dynamic control of internal forces was later addressed in [25]. More recently, compliant multi-contact behaviors using optimal distribution of contact forces has been explored [8]. In [20], the authors present an in-depth analysis of the interplay between CoM and internal multi-contact behavior in the context of compliant control of legged robots.

1.3 New contributions

Our motion planning strategy, initially proposed in [19], is a departure from these previous methods as we tackle the non-linear dynamical processes associated with extreme maneuvers in challenging terrains using numerical integration. Numerical integration allows us to approximate the solution to these non-linear processes given certain boundary conditions. This lets us understand CoM behaviors for any dynamically feasible motion.

The pipeline for our motion planning technique can be broken down algorithmically into a few phases. These phases are: (1) geometric planning based on desired motion, (2) generation of CoM dynamics through numerical integration, and (3) actively locating step transitions points. Geometric planning consists of selecting initial kinematic parameters. These parameters are restricted only by the dynamic limitations of the physical system. Next, dynamical equations of motion for the CoM (usually non-linear) are developed from which an approximation for CoM behavior (specifically state-space

behavior) can be calculated using numerical integration. These equations are generated using inverted pendulum dynamics and are augmented with a Multi-Contact Matrix for phases in which there is more than one point of supporting contact. Lastly, using the predicted CoM behavior, we can find step transition sequencing for maneuvers involving both single and multi-contact models while also ensuring contact constraints are upheld.

1.4 Structure of thesis

Chapter 1 gives a general overview of the goals of our lab as well as the direction of our research in motion planning and multi-contact state modeling. It also includes a brief overview of ongoing research as well as a description of the new contributions this thesis makes to the robotics community.

Chapter 2 covers the fundamental mathematics behind a new motion planning algorithm. This includes a detailed description of how we reduce the non-linear multivariate equations of motion often associated with dynamic locomotion to a non-linear ordinary differential equation which we propose to solve using numerical estimation techniques. It also outlines the pipeline used to automatically generate state-space CoM behavior for given motions.

Chapter 3 explains how to use the CoM behavior developed from the algorithms of the previous chapter to determine step transitions for the purpose of generating full motion sequences. It also includes a case study which validates our planning methods through comparison with the locomotion behavior of a human subject.

Chapter 4 presents the Multi-Contact Model first introduced in [20]. It has the capacity to incorporate internal tension forces during multi-contact configurations into the dynamic properties of the system. This makes the model a crucial component for analyzing complex maneuvers involving multi-contact phases.

Chapter 5 describes two case studies of maneuvers involving multi-contact states. The first study investigates the dynamics involved in an extreme swinging motion, specifically looking at tension forces and their feasibility based on reaction forces and friction cones at points of contact. The second study analyzes an extreme leaping maneuver and aims to predict takeoff and landing points as well as system dynamics by synthesizing multi-contact and single contact behaviors into one motion planning method.

Chapter 6 summarizes the contributions of this thesis. This includes a new motion planning strategy for non-linear dynamic systems formulated around numerical approximations and insights into the role of internal tension forces during multi-contact states. It also provides ideas for future study in the area of motion planning during both single and multi-contact phases.

The **Appendices** present supporting studies investigating the effect of moments about the CoM during locomotion planning. They also present recent work, expanding the concepts associated with motion planning and multi-contact dynamics originally developed for legged systems, and applications to case studies in brachiation and climbing maneuvers in which the CoM is located below the point or points of contact.

Chapter 2

Numerical Integration Algorithm

This chapter covers the fundamental mathematics behind calculating automatically generated phase curves for the locomotion of robots in rough terrain. These curves are the basis for the motion planning algorithm proposed in this thesis. First, the dynamics associated with the single point of contact model are developed. The numerical integration method is then introduced. Finally, the synthesis of the single contact dynamic model and numerical integration allows for the creation of automatically generated predictive phase portraits of CoM behavior.

2.1 Dynamic behavior of single contact point model

According to the principles of dynamic equilibrium, the sum of all moments acting on a moving system is equal to the net inertial moment. Given a simple system like the one shown in Figure 2.1, we can use this principle to generate the following moment balance expression that represents it,

$$\sum_{i=1}^{n_s} p_{cop_i} \times f_{r_i} + \sum_{i=1}^{n_s} m_{r_i} = p_{com} \times \Big(f_{com} + M\, g \Big) + m_{com}, \qquad (2.1)$$

where p_{cop_i} is the i-th foot contact pressure point (with respect to the coordinate origin); n_s is the number of supporting limbs; f_r and m_r are the reaction

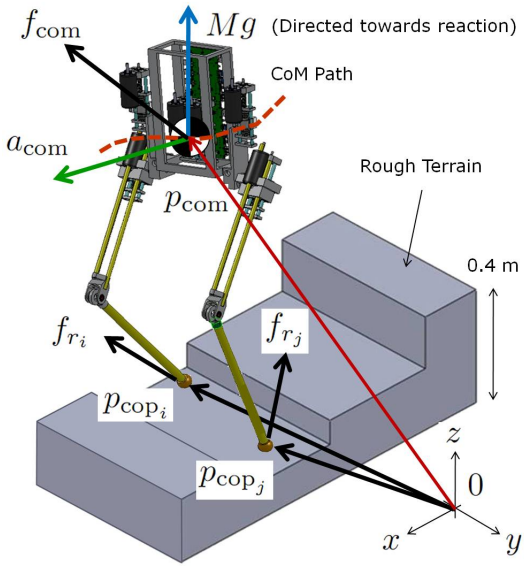

Figure 2.1: **Parameter depiction:** This figure defines the coordinates of the center of mass (CoM), center of pressures (CoP), and their position coordinates, p_{com}, p_{cop_i}, p_{copj}. The figure also depicts the reaction forces, f_{r_i}, f_{r_j} and the CoM's acceleration, a_{com}.

forces and moments at each pressure point; p_{com} is the location of the CoM (with respect to the coordinate origin); f_{com} amd m_{com} are the net force and moment acting on the CoM; M is the total mass of the system and g is the gravitational constant expressed in the positive vertical direction.

To simplify the complexity of this problem, for now, a system with only a single point of contact support at any given time will be considered. Eq. (2.1) can then be rewritten in the following form,

$$p_{cop_k} \times f_{r_k} + m_{r_k} = p_{com} \times \Big(f_{com} + M\, g \Big) + m_{com}, \tag{2.2}$$

where, k is the limb in contact with the terrain and p_{cop_k} is the limb's center

of pressure (CoP). Another simplifying assumption applied to the system to reduce its complexity is to consider only a planar model consisting of the vertical and frontal directions. The frontal direction will be labeled as the positive x-axis and the upward vertical direction will be labeled as the positive z-axis.

Using the single support model, the dynamic equilibrium of forces can be written as,

$$f_{r_k} = f_{com} + M\,g. \tag{2.3}$$

This can be substituted into Eq. (2.2) and then rearranged as,

$$(p_{com} - p_{cop_k}) \times f_{r_y} = m_{com}. \tag{2.4}$$

This vectorial representation can be rewritten into a system of three equations as follows,

$$f_{r_z}(p_{com_y} - p_{cop_{ky}}) - f_{r_y}(p_{com_z} - p_{cop_{kz}}) = m_{com_x} \tag{2.5}$$

$$f_{r_x}(p_{com_z} - p_{cop_{kz}}) - f_{r_z}(p_{com_x} - p_{cop_{kx}}) = m_{com_y} \tag{2.6}$$

$$f_{r_y}(p_{com_x} - p_{cop_{kx}}) - f_{r_x}(p_{com_y} - p_{cop_{ky}}) = m_{com_z}. \tag{2.7}$$

Since, for now, only the frontal-vertical plane is of interest, Eq. (2.6) is the only equation of the three that will currently be examined. Solving this equation for the position of the CoP leads to the following solution,

$$p_{cop_{kx}} = p_{com_x} - \frac{f_{r_x}}{f_{r_z}}\Big(p_{com_z} - p_{cop_{kz}}\Big) - \frac{m_{com_y}}{f_{r_z}}. \tag{2.8}$$

Using Newton's second law, force can be represented in terms of mass and acceleration (i.e., $f_{r_{kx}} = Ma_{com_x}$, and $f_{r_{kz}} = M(a_{com_z} + g)$). This lets the above equation be rewritten as,

$$a_{com_x} = \frac{\big(p_{com_x} - p_{cop_{kx}}\big)\big(a_{com_z} + g\big) - \frac{m_{com_y}}{M}}{\big(p_{com_z} - p_{cop_{kz}}\big)} \tag{2.9}$$

or,

$$a_{com_x} = \frac{\big(p_{com_x} - p_{cop_{kx}}\big)\big(a_{com_z} + g\big)}{\big(p_{com_z} - p_{cop_{kz}}\big)} - \frac{m_{com_y}}{M\big(p_{com_z} - p_{cop_{kz}}\big)}. \tag{2.10}$$

While these equations represent only the frontal-vertical plane, the same process could be used to find similar equations for the lateral-vertical and lateral-frontal planes.

2.2 Integration of geometric path

If we assumed that $a_{com_x} \triangleq \ddot{p}_{com_x}$, then this implies that Eqs. (2.9) and (2.10) are dynamic and non-linear. This non-linearity poses a major challenge stemming from the fact that it has no closed form solution. The study presented in this chapter corresponds to the specific situation where a_{com_x} and $\ddot{p}_{com_x}$ are time varying.

Since tackling this type of problem is not easy, the majority of work leading up to now has dealt with the problem by constraining the CoM trajectories to a fixed, level height (i.e. $p_{com_z} = \text{constant}$). This type of solution has led to the concept of the *Zero Moment Point*. While this solution does yield usable results, it is limiting. Two immediately recognizable limitations

are (1) the inability for the robot's CoM to mimic the path of a rising and falling human CoM during locomotion and (2) the inability to traverse rough environments in which the CoM must move up and down in order to satisfy the physical constraints of the robot and of the terrain. For this reason, the next contribution of this chapter is on predicting the behavior corresponding to the general case of Eq. (2.10). Numerical integration will be the new technique applied to accomplish this.

In order to use numerical integration, Eq. (2.10) needs to be manipulated such that a_{com_x} can be represented as a function of only p_{com_x}, p_{cop_x} and p_{cop_z}. During each step, however, the CoP location does not change since we assume that the foot remains stationary. This means that after some substitutions, an equation can be found that expresses a_{com_x} as a function of only p_{com_x} which is changing in time. To do these manipulations, first a dependency between p_{com_x} and p_{com_z} must be created. This is done by seeding a preselected geometric CoM path. This path selection is limited only by the physical constraints of the system. It can be chosen to mimic biological patterns, minimize mechanical and electrical power consumption, ensure kinematic and physical constraints are upheld or to satisfy any other factors. It is this freedom of choice that makes this contribution so valuable.

First, staying within kinematic constraints will be the foundation for selecting CoM paths, and for simplicity the path will be chosen to be a sequence of continuous (intersecting) piecewise linear functions. Given this assumption, p_{com_z} can be written as a function of p_{com_x} along with some slope a and offset

b as follows,

$$p_comnz = \begin{cases} a_1\, p_{com_x} + b_1, & p_{com} \in \mathbb{P}_1 \\ a_2\, p_{com_x} + b_2, & p_{com} \in \mathbb{P}_2 \\ \vdots & \\ a_N\, p_{com_x} + b_N, & p_{com} \in \mathbb{P}_N \end{cases} \tag{2.11}$$

where $\mathbb{P}_k$ represents the path of the CoM over step k. From this point, by simply differentiating each segment twice, thusly,

$$p_{com_z} = a_i\, p_{com_x} + b_i \;\Rightarrow\; a_{com_z} = a_i\, a_{com_x}, \tag{2.12}$$

the acceleration profile can be extracted. Next, expressions for p_{com_z} and a_{com_z} from Eqs. (2.11) and (2.12) are substituted into Eq. (2.10), giving the following result,

$$a_{com_x} = \frac{\Big(p_{com_x} - p_{cop_{kx}}\Big)\Big(a_i\, a_{com_x} + g\Big)}{\Big(a_i\, p_{com_x} + b_i - p_{cop_{kz}}\Big)} - \frac{m_{com_y}}{M\Big(a_i\, p_{com_x} + b_i - p_{cop_{kz}}\Big)}. \tag{2.13}$$

Here, a_{com_x} appears on both sides of the equation. Therefore it can be rearranged such that a_{com_x} ends up alone on the left hand side as follows,

$$a_{com_x} = \frac{\Big(p_{com_x} - p_{cop_{kx}}\Big) \cdot g}{\Big(b_i + a_i\, p_{cop_{kx}} - p_{cop_{kz}}\Big)} - \frac{m_{com_y}}{M\Big(b_i + a_i\, p_{cop_{kx}} - p_{cop_{kz}}\Big)}. \tag{2.14}$$

Notice that if (1) the CoP remains constant during each step and (2) the moments about the CoM are known, the above equation is of the form $\ddot{x} = \beta\,(x - \alpha) - \gamma$, which is linear and, as such, has closed-form solution.

However, the value of this contribution, again, is the fact that this method can handle kinematic paths that do not necessarily map to piecewise

linear functions but rather are based on more complex mappings. At first, for these more complex mappings, a point mass will be assumed which eliminates the moments about the CoM. With this assumption, an efficient gait produced by following circular arcs, i.e., $p_{com_z} = \left(r^2 - p_{com_x}^2\right)^{0.5}$ can be examined. In this case, path accelerations for a given step can be expressed by differentiating the arc. i.e.,

$$\begin{aligned} a_{com_z} = &- \left(r^2 - p_{com_x}^2\right)^{-1.5} p_{com_x}^2 \, v_{com_x}^2 \\ &- \left(r^2 - p_{com_x}^2\right)^{-0.5} v_{com_x}^2 \\ &- \left(r^2 - p_{com_x}^2\right)^{-0.5} p_{com_x} \, a_{com_x}, \end{aligned} \tag{2.15}$$

where, r is the radius of the arc. Plugging the above position and acceleration dependencies into Eq. (2.10) and rearranging as was done in the linear piecewise case (but without the moment term), the result is the following,

$$a_{com_x} = \left(p_{com_x} - p_{cop_{kx}}\right) \frac{N\left(p_{com_x}, v_{com_x}, p_{cop_{kx}}\right)}{D\left(p_{com_x}, p_{cop_{kx}}, p_{cop_{kz}}\right)}, \tag{2.16}$$

with,

$$N \triangleq g - \left(r^2 - p_{com_x}^2\right)^{-1.5} p_{com_x}^2 \, v_{com_x}^2 - \left(r^2 - p_{com_x}^2\right)^{-0.5} v_{com_x}^2 \tag{2.17}$$

$$D \triangleq \left(r^2 - p_{com_x}^2\right)^{0.5} - p_{cop_{kz}} + \left(p_{com_x} - p_{cop_{kx}}\right)\left(r^2 - p_{com_x}^2\right)^{-0.5} p_{com_x}. \tag{2.18}$$

The acceleration of Eq. (2.16) is non-linear and, therefore, no longer has a closed-form solution.

If the CoM geometric paths are generated by a more sophisticated planner with more complex kinematic dependencies and there are no moments about the CoM, the acceleration profile will be non-linear with general expression,

$$a_{com_x} = \Big(p_{com_x} - p_{cop_{kx}}\Big) \cdot \Phi\Big(p_{com_x}, v_{com_x}, p_{cop_{kx}}, p_{cop_{kz}}\Big), \tag{2.19}$$

or, with the inclusion of moments,

$$a_{com_x} = \Big(p_{com_x} - p_{cop_{kx}}\Big) \cdot \Phi\Big(p_{com_x}, v_{com_x}, p_{cop_{kx}}, p_{cop_{kz}}, m_{com_y}\Big), \tag{2.20}$$

where, $\Phi(\cdot,\cdot,\cdot,\cdot)$ and $\Phi(\cdot,\cdot,\cdot,\cdot,\cdot)$ are non-linear functions, and as such, do not have closed-form solutions.

2.3 State-space behavior prediction

The objective of this section is to show how to extract state-space trajectories for arbitrary geometric CoM paths, $\mathbb{P}_k$. The difficulty comes in trying to solve non-linear differential equations such as Eqs. (2.19) and (2.20). To do, this we employ numerical integration. Numerical methods can approximate the solution to a problem that does not have an exact solution or has an exact solution but which is too complex to solve analytically. They do this by looking into the results of a related problem that has an easy to calculate, solution. In the case of Eq. (2.19), accelerations are known as a function of CoM location in the frontal direction, CoP position in the frontal-vertical plane and CoM velocity in the frontal direction. Given this data, approximations can be made for the CoM path trajectory versus velocity (i.e. the state-space trajectory).

For the sake of simplicity, we consider the case of a piecewise linear CoM trajectory and we let $x \triangleq p_{com_x}$ allowing Eq. (2.19) to be represented as,

$$\ddot{x} = f(x, \dot{x}), \tag{2.21}$$

where $f(x, \dot{x})$ is the RHS of Eq. (2.19) and CoP location is considered to be constant over each step. This representation can also be used for Eq. (2.20) if we assume that moments are known at all times. The simplifying assumption being made when using numerical integration is that over very small iterations of x, the acceleration of the CoM, $\ddot{x}$, and velocity of the CoM, $\dot{x}$, remain constant. Using this assumption, it is possible to approximate the change in CoM position over a time-step, ϵ (the perturbation), given initial conditions $(x_k, \dot{x}_k)$ and approximate the behavior at neighboring points as,

$$\dot{x}_{k+1} \approx \dot{x}_k + \ddot{x}_k \epsilon, \tag{2.22}$$

$$x_{k+1} \approx x_k + \dot{x}_k \epsilon + 0.5\, \ddot{x}_k \epsilon^2. \tag{2.23}$$

From Eq. (2.22) an expression of the perturbation in terms of the velocities and acceleration can be found $\epsilon \approx (\dot{x}_{k+1} - \dot{x}_k)/\ddot{x}_k$, and substituting $\ddot{x}_k = f(x_k, \dot{x}_k)$ into Eq. (2.23) yields,

$$x_{k+1} \approx \frac{\left(\dot{x}_{k+1}^2 - \dot{x}_k^2\right)}{2\, f\left(x_k, \dot{x}_k\right)} + x_k, \tag{2.24}$$

which is the state-space approximate solution that is desired.

The pipeline for finding state-space trajectories is as follows: (1) choose a very small time perturbation, ϵ, (2) given known initial CoM velocity, $\dot{x}_o$,

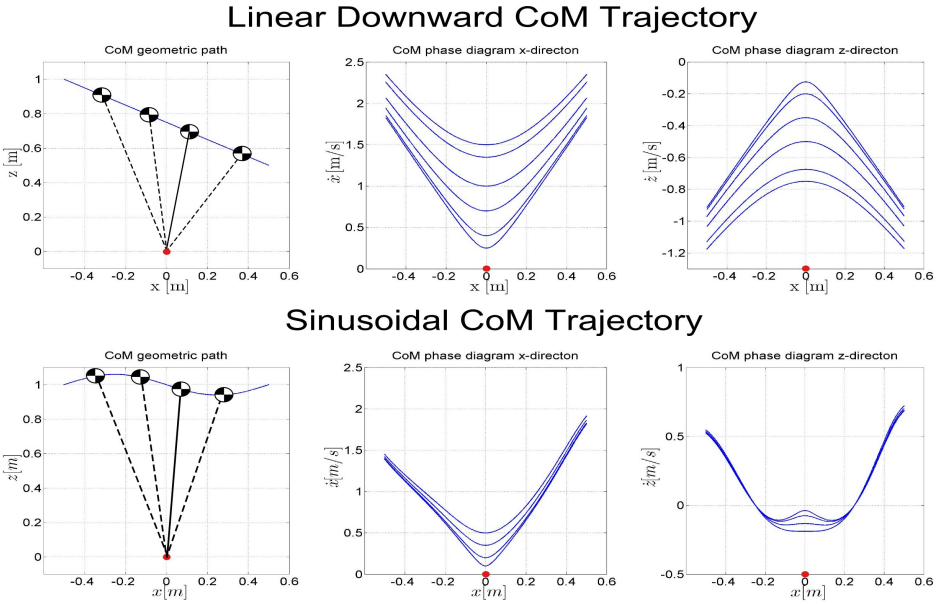

Figure 2.2: **Prediction of CoM behavior using numerical integration:** These phase diagrams correspond to Matlab simulations of CoM behavior given a foot contact point (the origin), a desired CoM kinematic path (straight line and sinusoid), and varying boundary conditions given at the apex of the step (x-direction velocity when the CoM is directly above the foot contact point).

initial CoM position, x_o, and constant CoP location, use Eq. (2.19) to calculate initial acceleration, $\ddot{x}_o$, (3) get neighboring velocity, $\dot{x}_{k+1}$, using Eq. (2.22), (4) using Eq. (2.24) get the next position x_{k+1}, (5) plot the point $(x_{k+1}, \dot{x}_{k+1})$ in the phase-plane, (6) repeat steps (1) through (5). Notice that we can iterate both forward and backward in time. For backward recursion, a negative perturbation, ϵ, needs to be used.

In Figure 2.2, this pipeline is applied to two different trajectories, one where the CoM follows a downward linear path (top row) and another where

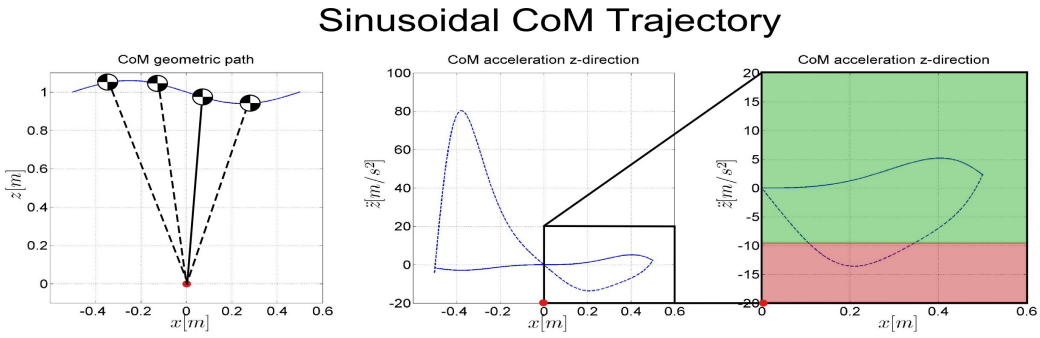

Figure 2.3: **Comparison of feasible and infeasible CoM trajectories:** These plots depict the CoM geometric path (left), z-direction acceleration (center) and an enlarged plot of z-direction acceleration for two centers of mass following the same sinusoidal path but having differing apex velocities (right). The dashed line represents the trajectory with a larger apex velocity. The red and green areas, respectively, represent the regions where accelerations in the z-direction are less than or greater than the acceleration due to gravity.

the CoM follows a sinusoidal wave (bottom row). In both cases, the contact foot is located at point $\left(p_{cop_x}, p_{cop_z}\right) = (0, 0)[m]$. For both studies, various boundary conditions are provided at the apex (i.e., when the CoM is over the contact point) corresponding to the CoM velocity in the x-direction at that point.

Looking further into the behavior of the CoM while following a sinusoidal path, specifically the accelerations in the z-direction, we can see that it is possible to rule out some boundary conditions that lead to force profiles that cannot be fulfilled. Figure 2.3 contains plots of the geometric path and acceleration profile of two centers of mass following the same sinusoidal path as in Figure 2.2 but with the dashed line having a larger apex velocity than the solid line. If it is assumed that the point of contact is not pinned to the

ground, then we can say that it is impossible for the CoM to have an acceleration in the z-direction that is more negative than the acceleration due to gravity at any point. The red area in the enlarged plot on the right depicts the region that must be avoided to ensure that the foot is alway pushing into the ground and never pulling away from it, as this would cause the leg to lose contact. The dashed line clearly enters this region telling us that following the given geometric path with that given apex velocity is not feasible.

If the trajectories and boundary conditions pass this initial test, from there cascading phase curves can be generated and used to plan step transition points for a multi-step motion sequence. The details of this process are discussed in the next chapter.

Chapter 3

Dynamic Rough Terrain Locomotion

Equipped with the numerical integration method it is possible to plan dynamic walking in very rough terrains. Here, a clear pipeline is given for the automatic motion planning sequence: (1) develop a continuous CoM geometric path to overcome the terrain, (2) select foot contact locations for each step, (3) choose boundary conditions, i.e., velocities for the CoM at step apexes, (4) using Eqs. (2.22) (2.23) and (2.24), predict phase curves for each step and (5) find the intersections between the phase curves of neighboring steps which represent the phase point where the transition between contacts needs to occur. The resulting multi-step phase diagram is the locomotion plan that can be fed into a control stage.

For simplicity, the term associated with moments about the CoM such as the one present at the end of Eqs. (2.10), (2.13) and (2.14) will be eliminated through the assumption that every system has a point mass. Refer to Appendices A, B and C for more details regarding the study of the effect of moments about the CoM during motion planning.

3.1 Phase Intersections to determine step transitions

Here, an example that demonstrates the pipeline for finding the step transition location between two subsequent steps, specifically the case shown in Figure 3.1 where a circular arc trajectory is followed by a straight line trajectory, is examined. The motivation behind using different curves is to illustrate the versatility of the method for working with any CoM path. The position of the first and second foot contact locations are shown as red circles. The center graph depicts the phase curves for the first and second steps calculated based on boundary conditions for the CoM at the apexes equal to $(x_0, \dot{x}_0) = (0, 0.6)$ and $(x_1, \dot{x}_1) = (0.4, 0.45)$. The pictures of the human are only to illustrate the switching strategy between steps but have not been used to derive CoM geometric paths for this particular example.

Because the perturbation method of Eq. (2.24) is numerical, it is not obvious how to derive the intersection point between CoM phases. Our approach is as follows, (1) fit a polynomial of order 5 using Matlab's `polyfit()` function, to each of the two CoM phases, (2) subtract the two polynomials and find its roots using Matlab's `roots()` function, (3) discard imaginary roots, (4) get the point of intersection within CoM position range, and (5) extract the CoM velocity intersection by evaluating the polynomial at the CoM position intersection. If we apply this pipeline to the example of Figure 3.1, we find the step intersection is located at $(x_s, \dot{x}_s) = (0.3, 0.7)$.

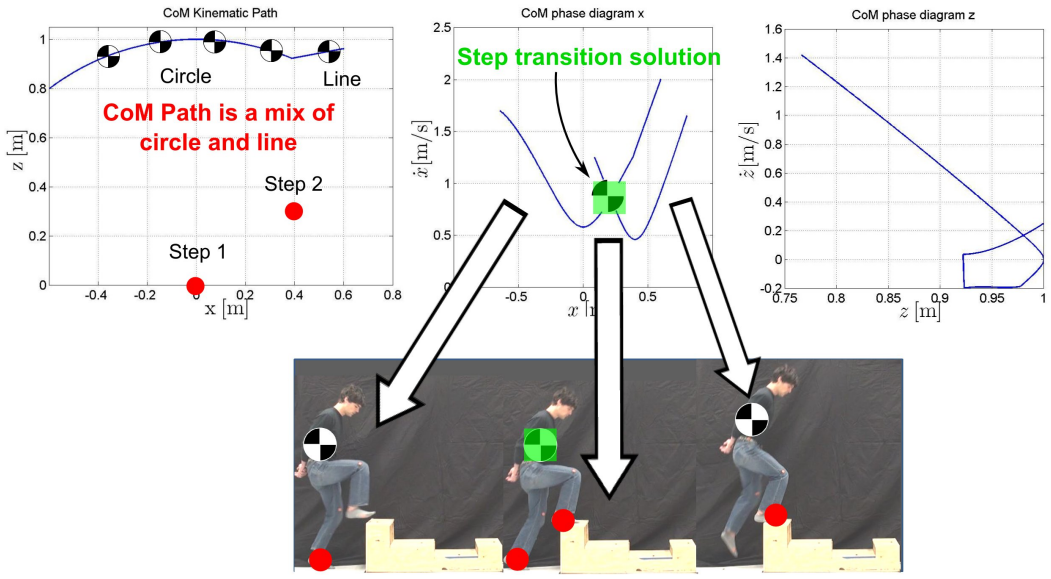

Figure 3.1: **Step solver:** The center graph depicts phase curves for the two steps given the CoM path shown on the left. We fit polynomials and find the differential root between the adjacent curves to find the point of intersection.

3.2 Methods for validation experiment

In this section, we present a case study aimed at matching the motion pattern of a human subject for the purpose of validating this motion planning algorithm. In the study, we use a stair-like terrain shown in Figures 3.2 and 3.3 consisting of four steps of varying heights that simulates a rough environment that is challenging to navigate yet still traversable by a human using only the feet as supporting contacts. Until this contribution, there had been no method for planning biped locomotion over this type of terrain at high speeds. In the following section, the input parameters for our motion planning algorithm will be chosen to match those of a human walking over this artificial terrain. From

there it will be possible to compare the state-space phase plot taken directly from the motion of a human subject and compare it to the one automatically generated using numerical integration. Finally, we show that there is a strong correlation between the phase plot of the human and the automatically generated phase plot.

3.2.1 Capturing human terrain traversal data

To find the locomotion parameters for the motion of a human traversing the stair-like terrain, data was first collected through a manual motion capture method. A video camera was set up in the HCR lab and used to record the locomotion of a human subject. It is assumed that the camera was located far enough from the subject that the recordings are of pure planar motion with negligible lens distortion. The maneuver studied included 7 steps and lasted approximately 6.5 seconds. Although the raw motion capture video was taken at 30 frames per second, only every 3^{rd} frame was used in order to reduce the amount of data needing to be processed. This made the sampling rate effectively 10 frames per second and therefore 65 frames were included in this analysis.

Once the video was recorded, the position of the CoM and the location of the feet during points of supporting contact in each frame were extracted. This was done in Matlab using its `ginput()` command. This command allows frames to be loaded individually and displayed. The command then records user selected pixel locations chosen, using the mouse, on the image. In each

frame included in this analysis, 15 points were selected corresponding to the location of the centers of mass of 14 individual body segments as well as 1 more for the point of supporting contact. Given the total mass of the human subject, estimates for the mass of each body segment were compiled using data from [27] that gives body segment masses as a percentage of a human's total mass. The location of the center of mass in each body segment was taken from the same paper and markers were applied to the subject at those places. The 14 markers were split up as follows: 2 on each foot, calf, thigh, upper arm, forearm and hand plus 1 each for the head (head and neck) and the torso (pelvis, abdomen and chest). Using these body segment CoM locations along with their relative masses, a vectorial weighted sum was calculated that generated the location of the CoM of the entire human subject, p_{com}. By using this CoM calculation approach rather than simply tracking a single point on the subject's abdomen, more accurate as well as less noisy data for the subject's CoM trajectory was obtained. The supporting contact location for each step, p_{cop_k}, was taken directly from `ginput()` data.

Matlab's `cftool()` function was used to generate a best fit curve for the p_{com} data and also generate values for its first and second derivatives (CoM velocity and CoM acceleration). The CoM path, foot contact locations, and velocity plots are shown in Figure 3.2. Also, the phase diagram of the human motion is shown by the solid orange line in Figure 3.4.

Having created the state-space phase plot for the motion of the human subject, the next step was to generate phase curves and step transition points

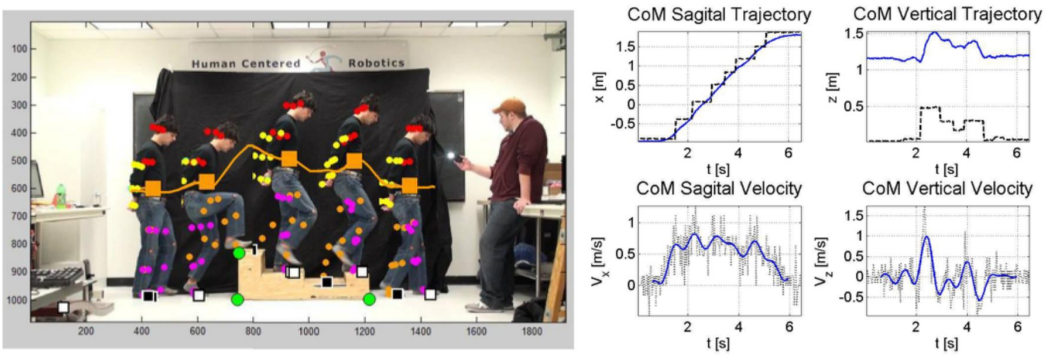

Figure 3.2: **Data extraction from human walk:** A human subject walks over a rough terrain. Marker tracking is implemented and used to extract approximate CoM paths as well as CoM trajectories and velocities in the x-direction and z-direction.

automatically and compare them to the data collected from the human. This was done using the numerical integration pipeline described at the beginning of this chapter. Foot contact locations were taken directly from the motion capture process, apex velocities were chosen to be the same as the velocities of the human subject while at the apex of each step and the geometric CoM trajectory was chosen to be modeled by a sequence of linear piecewise functions that approximate the actual path that the human subject's CoM followed.

3.2.2 Validation experiment results and analysis

Using the human based input parameters, the motion planning pipeline was executed and an automatically generated phase diagram was created. The results of these calculations are depicted in Figure 3.3. The snapshots on the upper left show a mixed reality sequence derived from the planner. Time trajectories of CoM frontal and vertical behavior are shown to the right and

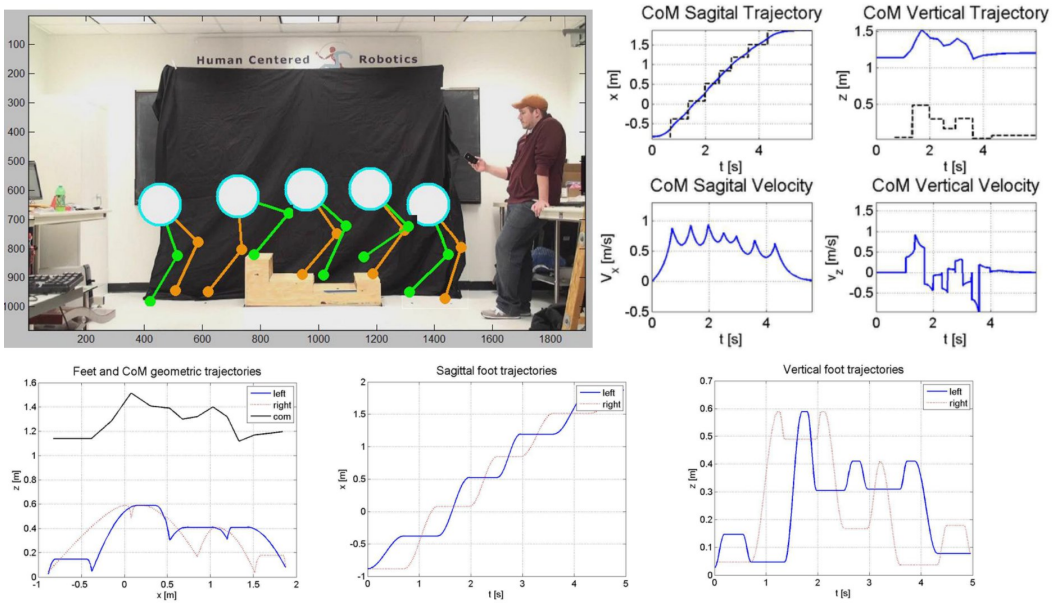

Figure 3.3: **Automatic locomotion planner:** The figure in the upper left shows a mixed reality and artificial image based on the kinematic data generated in the automatic motion planner. Data for the CoM is shown in the four figures in the upper right while feet trajectories are depicted in the three plots along the bottom.

are derived from the phase curves. A separate planner computes basic foot trajectories to synchronize with CoM behavior and switch step at the desired contact intersections.

In Figure 3.4 the automatic and human phase curves are compared for two separate sets of input parameters. The top plots show the kinematic trajectory of the human CoM (derived using motion capture) versus a piecewise linear approximation that was used in the automatic walking simulation. Here, the red dots correspond to the position of the foot contacts. The bottom figure shows Matlab plots of x-direction phase curves for the human and the

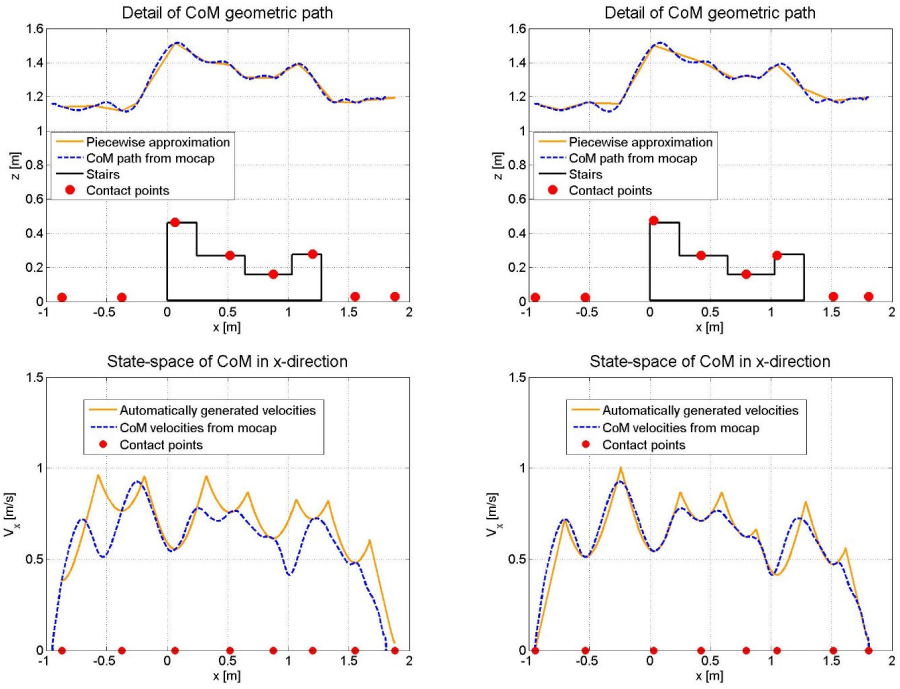

Figure 3.4: **Human and automatic phase portraits:** These plots show the geometric and state-space plots (top and bottom respectively) for both the human data collected via motion capture and the automatically generated data from the motion planning algorithm. The plots on the left show the results obtained using the initial foot contact locations as inputs. The plots on the right show the results obtained using the adjusted foot contact location as inputs, chosen via the process described in the text.

automatic simulation. The plots on the left were developed first based on the locations of the contact points obtained from the motion capture process. Apex CoM positions and velocities (boundary conditions) were extracted based on these contact positions. Looking at the state-space plot associated with these inputs, one can see a general trend in the automatically generated data that resembles the human data. We noticed, though, that slight adjustments in

the contact locations (maximum ± 5[cm] in the x-direction) could cause the automatically generated data to move toward a better correlation with that of the human as seen in the plots on the right in Figure 3.4. We believe that this is a valid adjustment due to our assumption that the contact is a point contact with no ankle-like element. It is impossible for a human to walk with true point contact behavior due to physical limitations such as foot geometry and muscular strength and it is also very difficult to eliminate the use of the ankle. For these reasons, the center of pressure of the system will constantly be moving and cannot be precisely measured using our motion capture technique. Thus, it seems reasonable to assume that these slight changes to the input CoP location are just as valid as the ones taken directly from the motion capture process. We also notice that the phase plots of the human have a smooth pattern. This is due to the smoothening effect of dual contact during the stance phase. This is not the case during the automatic walk because we have neglected the dual contact phase and, therefore, the transitions between contacts are instantaneous.

The strong correlation between the automatically created phase curves and the human's phase curves, especially after adjusting the contact points, demonstrates the validity of the motion planning algorithm presented in this chapter. From here, it is possible to select input parameters that satisfy any desired requirements. This allows researchers to try different potential foot placements, apex velocities and CoM paths to see if the resulting motion plan is possible based on the physical constraints of a certain robot.

There is no need to limit this technique to only locomotion. In fact, the same principle of numerical integration can be applied to more complex maneuvers. These actions, though, usually require more than a single point of contact which, up to this point, has not been accounted for in this thesis. In order to transition the single contact model to a multi-contact model, a special matrix called the Multi-Contact Matrix (introduced in [20]) must be employed. With this new tool, almost any motion, including extreme maneuvers like those executed during the sports of freerunning and parkour can be analyzed and planned for.

Chapter 4

The Multi-Contact Model

While simplifying the locomotion problem to a series of steps involving only single points of contact makes motion planning easier, that model limits possible CoM kinematics to unnatural basic behaviors. However, by adding the concept of multi-contact states, a vast new set of maneuvers becomes feasible. Planning can even be done for complex, acrobatic motions like those freerunners make while traversing over and around obstacles in urban environments, which will be referred to as *extreme maneuvers*.

4.1 Description of the Multi-Contact Matrix

When considering multi-contact states, the Multi-Contact Matrix must be implemented in addition to the methods used for the single contact model. The Multi-Contact Matrix, developed in [20], describes the complex interactions between contact forces and CoM behavior and is founded on the principle of dynamic equilibrium. Based on this study, a virtual linkage model is proposed for humanoid robots to analyze the interdependencies between whole-body contacts and CoM behavior.

Consider the situation shown in Figure 4.1 where the human subject is

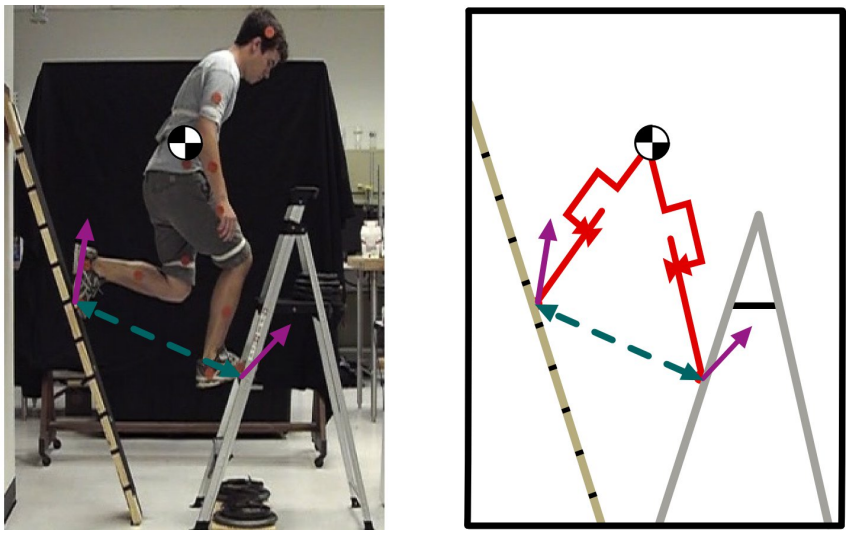

Figure 4.1: **Multi-Contact stance:** On the left we see the human subject suspended over two points of contact. One foot is on the sloped board and the other is on the ladder rung. The figure on the right is a representation of the same system where the legs are modeled as prismatic actuators. The blue dashed line represents the internal tension forces between the contacts while the purple vectors represent the respective reaction forces at each foot. The Multi-Contact Matrix is used to calculate these reaction forces based on CoM behavior and internal tension forces.

supported by two feet. For simplicity, the feet are modeled as point contacts. In such a case, the Multi-Contact Matrix can be derived from the virtual linkage model as,

$$\begin{pmatrix} f_{com} + Mg \\ m_{\text{com}} \\ f_t \end{pmatrix} = C_{7\times 6} \begin{pmatrix} f_{r(RF)} \\ f_{r(LF)} \end{pmatrix}, \tag{4.1}$$

where $f_{r(RF)}$ and $f_{r(LF)}$ represent the three dimensional reaction forces on the right and left feet, respectively, $f_{com} \triangleq M\, a_{com}$ represents inertial forces caused by center of mass accelerations, a_{com} is the three dimensional vector of center

of mass linear accelerations, M is the total mass of the human, $g \triangleq (0, 0, 9.81)$ is the vector of gravitational accelerations pointing upward to be consistent with reaction forces, m_{com} is the three dimensional vector of inertial moments at the center of mass, and f_t is the one dimensional vector of internal tension forces between the feet.

In the above equation, $C_{7\times6}$ seems like it could be the Multi-Contact Matrix we need, however, it does not fully describe the relationship between CoM behavior and reaction forces. This is evident by the non-square nature of $C_{7\times6}$. Non-square matrices are non-invertible and, therefore, the form of the Multi-Contact Matrix in Eq. (4.1) only allows mapping from reaction forces to CoM behavior and internal tensions. It cannot be used to map tensions and inertial forces to reaction forces as desired.

In the following section, the derivation of the virtual linkage model will be presented, followed by the simplifications used to transform the $C_{7\times6}$ matrix into a square $C_{6\times6}$ Multi-Contact Matrix that can be used to map tension and inirtial forces to reaction forces.

4.2 From virtual linkage to Multi-Contact Matrix

The $C_{7\times6}$ Matrix from Eq. (4.1) is derived using dynamic balance of moments and forces similar to the equations used in Section 2.1. The following relationship can be specified, which links inertial and gravitational behavior

to reaction forces (see [20] for the derivation of this model),

$$\begin{pmatrix} [I]_{3\times3} & [I]_{3\times3} \\ \hat{P}_{cop_1} & \hat{P}_{cop_2} \end{pmatrix} \begin{pmatrix} f_{r1} \\ f_{r2} \end{pmatrix} = \begin{pmatrix} [I]_{3\times3} & [0]_{3\times3} \\ \hat{P}_{com} & [I]_{3\times3} \end{pmatrix} \begin{pmatrix} f_{com} + Mg \\ m_{com} \end{pmatrix}, \quad (4.2)$$

where the operators with a $(\hat{.})$ correspond to the cross product matrix, p_{cop_i} corresponds to the center of pressure of the i-th foot and p_{com} corresponds to the position of the CoM. The internal forces can also be expressed as,

$$f_t = S_t \left({}^{VL}R_0 \right) \Delta_t \begin{pmatrix} f_{r1} \\ f_{r2} \end{pmatrix}, \quad (4.3)$$

where the differential operation is described by,

$$\Delta_t \triangleq \begin{pmatrix} -[I]_{3\times3} & [I]_{3\times3} \end{pmatrix}, \quad (4.4)$$

and the rotation matrix that transforms an inertial frame to the virtual linkage frame is,

$${}^{0}R_{VL} \triangleq \begin{pmatrix} (x_{VL} \cdot \hat{x}) & (x_{VL} \cdot \hat{y}) & (x_{VL} \cdot \hat{z}) \\ (y_{VL} \cdot \hat{x}) & (y_{VL} \cdot \hat{y}) & (y_{VL} \cdot \hat{z}) \\ (z_{VL} \cdot \hat{x}) & (z_{VL} \cdot \hat{y}) & (z_{VL} \cdot \hat{z}) \end{pmatrix}. \quad (4.5)$$

Calling,

$$\left[W_{com} \right]_{6\times6} \triangleq \begin{pmatrix} [I]_{3\times3} & [0]_{3\times3} \\ \hat{P}_{com} & [I]_{3\times3} \end{pmatrix}^{-1} \begin{pmatrix} [I]_{3\times3} & [I]_{3\times3} \\ \hat{P}_{cop_1} & \hat{P}_{cop_2} \end{pmatrix} \quad (4.6)$$

$$\left[W_{\text{int}} \right]_{1\times6} \triangleq S_t \left({}^{VL}R_0 \right) \Delta_t, \quad (4.7)$$

the result is a non-square multi-contact expression,

$$\begin{pmatrix} f_{com} + M\,g \\ m_{com} \\ f_t \end{pmatrix} = [C]_{7\times6} \begin{pmatrix} f_{r1} \\ f_{r2} \end{pmatrix}, \quad (4.8)$$

with,

$$[C]_{7\times 6} \triangleq \left(\begin{array}{c} \left[W_{com}\right]_{6\times 6} \\ \hline \left[W_{\text{int}}\right]_{1\times 6} \end{array}\right). \tag{4.9}$$

This $C_{7\times 6}$ matrix allows the forces and moments acting on the CoM as well as the tension forces between contact points to be calculated given reaction forces, as mentioned above. Because it is non-square, it is not invertible and therefore, it cannot be used in its current form to extract reaction forces from tensions, CoM forces and CoM moments. However, the fact that the matrix is non-square reveals that there is a redundancy on the RHS of the above equation. For this reason, an interdependency between inertial and reaction forces needs to be found. This is done by examining one of the natural principles of a system with only two contact points. Assuming that the CoM lies in a non-collinear location with respect to the two supporting contacts, forces can only be applied to the CoM in the plane defined by these those 3 points. This leads to the understanding that there can be no forces applied laterally and, therefore, there can be no accelerations in that direction either. These y-direction elements can be eliminated from the $C_{7\times 6}$ matrix though the use of the following selection matrix,

$$S_{\text{VL}} \triangleq \left(\begin{array}{c|c|c} \begin{matrix} 1 & 0 & 0 \\ 0 & 0 & 1 \end{matrix} & [0]_{2\times 3} & [0]_{1\times 3} \\ \hline [0]_{3\times 3} & [I]_{3\times 3} & [0]_{3\times 1} \\ \hline [0]_{1\times 3} & [0]_{1\times 3} & 1 \end{array}\right) \epsilon\, \Re^{6\times 7}. \tag{4.10}$$

With this selection matrix, the $C_{7\times6}$ can be changed into a matrix $\epsilon\,\mathcal{R}^{6\times6}$

$$[C]_{6\times6} \triangleq S_{\mathrm{VL}} \begin{pmatrix} \big[W_{com}\big]_{6\times6} \\ \hline \big[W_{\mathrm{int}}\big]_{1\times6} \end{pmatrix}. \tag{4.11}$$

This $C_{6\times6}$ matrix is now the Multi-Contact Matrix. It is square which (assuming it is non-singular) means it can be inverted, allowing for reaction forces to be solved for given inertial and tension forces.

4.3 Force and moment balance decomposition

Armed with the invertible Multi-Contact Matrix, Eq. (4.1) can be rearranged and written in the following form,

$$\begin{pmatrix} f_{r(RF)} \\ f_{r(LF)} \end{pmatrix} = C_{6\times6}^{-1}\, S_{\mathrm{VL}} \begin{pmatrix} f_{com} + Mg \\ m_{com} \\ f_t \end{pmatrix}. \tag{4.12}$$

Next, breaking down the inverted Multi-Contact Matrix as such,

$$C_{6\times6}^{-1} = \big(\, C_{f\,6\times2} \mid C_{m\,6\times3} \mid C_{t\,6\times1} \big)\,, \tag{4.13}$$

the more intuitive form of Eq. (4.12) can be expressed as,

$$\begin{pmatrix} f_{r(RF)} \\ f_{r(LF)} \end{pmatrix} = C_f\; S_{xz} \left(f_{com} + Mg \right) + C_m\, m_{com} + C_t\, f_t \tag{4.14}$$

where,

$$S_{xz} \triangleq \begin{pmatrix} 1 & 0 & 0 \\ 0 & 0 & 1 \end{pmatrix}, \tag{4.15}$$

is a subcomponent of S_{VL} that removes the y-direction. Eq. (4.14) will serve as the model used to both analyze and also synthesize extreme multi-contact maneuvers in the following chapter.

Chapter 5

Multi-Contact Locomotion

The focus of this chapter will be to show the use of the Multi-Contact Matrix in two case studies of different extreme maneuvers and why it is so important for calculating accurate reaction forces. In each case study, motion capture was taken of a human subject performing an extreme maneuver and CoM kinematics were extracted using the same techniques described in section 3.2.1.

5.1 The role of internal tension forces

There are an infinite combination of tension forces that allow a human to behave with any specified kinematics. The simplest case is to imagine a human remaining stationary while holding a railing with both hands. It is impossible to tell the reaction forces at the hands by simply noting the behavior of the CoM. The hands could be pushing toward or away from each other with any amount of force and the CoM would remain fixed if the forces applied at each hand are equal. In most cases, the range of possibilities can be reduced based on physical restrictions, namely friction at the points of contact and force generation capability.

With this understanding, Eq. (4.14) can be used to validate the feasibility of certain internal tension forces given specific contact locations and CoM kinematics. The following pipeline is used for this validation: (1) perform motion capture of multi-contact maneuver for generating artificial CoM kinematics, (2) calculate the Multi-Contact Matrix, (3) select internal tension profile based on force generation capability, (4) determine a friction cone at contact points, (5) use Eq. (4.14) to calculate reaction forces, and (6) check whether reaction forces fit within the measured friction cones.

Using this pipeline, different tension forces can be tested for specific situations and motions and the required reaction force necessary based on those tension forces can be found. If the reaction forces lie within the friction cone of the contact point, then the tension force being tested is feasible. If the reaction forces exceed the friction cone at any point, the tension forces being used are not feasible for the specified CoM behavior.

5.2 Extreme swinging maneuver

In this section, the maneuver depicted in Figure 5.1 is analyzed. Here, the human subject is suspended on two points of contact (one at each foot) and swings forward and backward. The upper left plot shows the CoM path while the two plots next to it show velocity and acceleration profiles in state-space. The plot on the lower right shows the tension force profile used to calculate the reaction forces shown in the two plots to its left. The tension forces were chosen based on an iterative approach where values that seemed intuitively

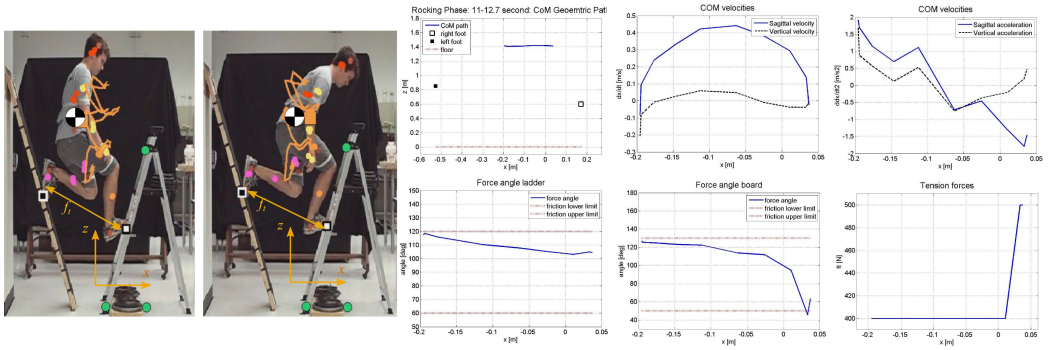

Figure 5.1: **Analysis and estimation of internal tensions during a swinging maneuver:** In this figure, we depict motion paths and state-space curves of captured motion of a multi-contact swinging behavior as well as estimation of internal tensions using the Multi-Contact Matrix.

reasonable were tried until values that caused the reaction forces to lie within their respective friction cones were found. Friction cone angles were found experimentally for the contacts of the ladder and angled board with the shoe sole of the human subject.

In this case, internal tension forces that oscillated between 400-500[N], generated reaction forces that lay within these friction cones. Again, these may not be the exact values of the tension forces exerted by the human during the swinging maneuver but they represent values of forces that could have been applied to created the same motion.

5.3 Extreme leaping maneuver

This case study focuses on the motion and forces involved in jumping from a lower ladder rung to a higher one as shown in Figure 5.2. In the

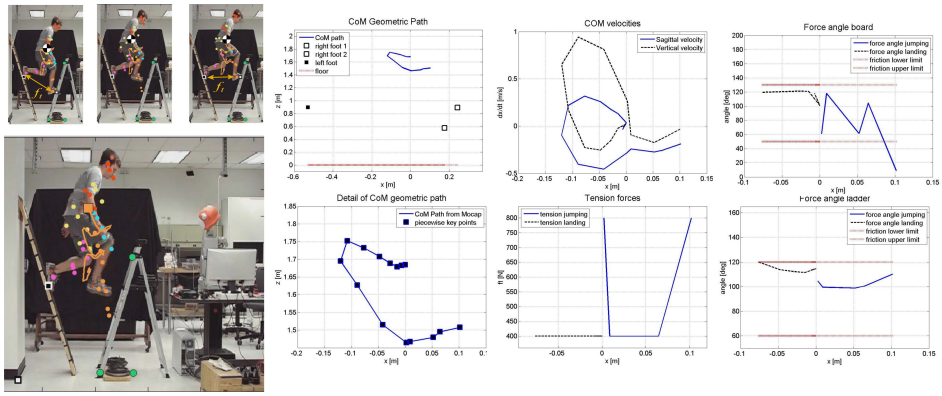

Figure 5.2: **Analysis and estimation of internal tensions during jumping and landing maneuvers:** In this figure, we depict a gap leaping maneuver and the extraction of data using motion capture devices.

images on the left, the human subject can be seen leaping from the 2^{nd} to the 3^{rd} rung of a ladder while maintaining a point of contact on a sloped board behind him. This maneuver can be broken up into 3 distinct segments: (1) a multi-contact takeoff phase, (2) a single contact flight phase, and (3) a multi-contact landing phase. The goal is to develop a technique for modeling this type of maneuver such that motion plans can be generated based on desired CoM kinematics. This includes testing feasibility of the flight path based on acceleration restrictions, locating points of takeoff and landing (i.e., the points where there is a shift between single contact and multi-contact), and testing to see that reaction forces lie within their respective friction cones.

5.3.1 Angle of attack analysis

First, restrictions on the flight phase will be discussed. Figure 5.3 shows two different CoM paths for the ladder leaping action. The left plot is based on

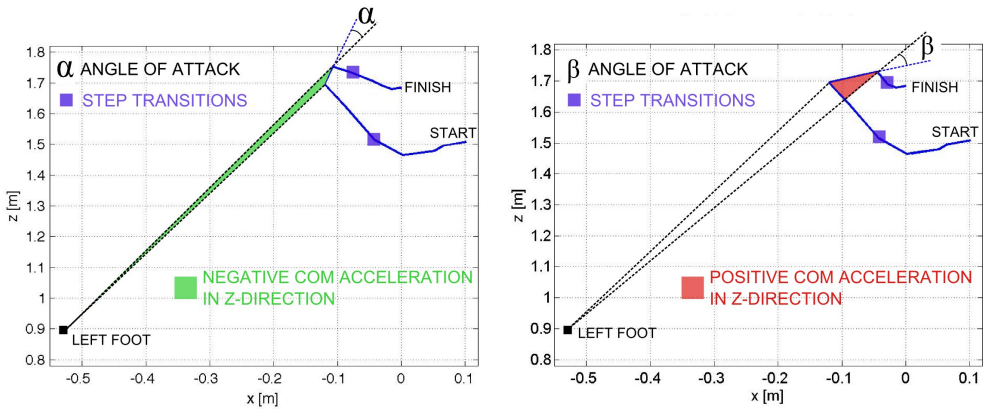

Figure 5.3: **Angle of attack for single contact phase:** In these graphs we show the angle of attack for two different center of mass geometric paths. Only the one on the left is feasible since its angle of attack is positive, i.e., $\alpha > 0$, resulting in a deceleration before reaching the vertical apex. On the other hand, the right graph has an angle of attack $\beta < 0$.

the motion capture data from the human subject while the right plot depicts an arbitrarily selected path. Next, we show that based on basic dynamic principles that must be satisfied during the single contact flight phase, the arbitrary path is not feasible while the human based trajectory is feasible.

In both cases shown in Figure 5.3, the CoM path is formed by a series of piecewise linear functions. For this reason, along with the fact that only the single contact flight phase is being studied, Eq. (2.14) can be considered. Since the CoM remains in front of the CoP for the entirety of the motion, the numerator of Eq. (2.14) will remain positive as well. Therefore, to determine orientation of the acceleration in the x-direction, only the sign of the denominator needs to be known which is only a function of CoP location (p_{cop}) and CoM path parameters (a_i, b_i). i.e.,

$$\text{if} \quad a_i\, p_{cop_x} + b_i > p_{cop_{kz}}, \quad \text{then} \quad a_{com_x} > 0$$

$$\text{elseif} \quad a_i\, p_{cop_x} + b_i < p_{cop_{kz}}, \quad \text{then} \quad a_{com_x} < 0$$

$$\text{else} \quad a_{com_x} \to \infty.$$

Using the equality $b_i = p_{com_z} - a_i\, p_{com_x}$, derived from Eq. (2.12), the above conditions can be rewritten as,

$$\text{if} \quad a_i < \frac{p_{com_z} - p_{cop_z}}{p_{com_x} - p_{cop_x}}, \quad \text{then} \quad a_{com_x} > 0$$

$$\text{elseif} \quad a_i > \frac{p_{com_z} - p_{cop_z}}{p_{com_x} - p_{cop_x}}, \quad \text{then} \quad a_{com_x} < 0$$

$$\text{else} \quad a_{com_x} \to \infty.$$

These manipulations show that if the slope a_i is smaller than the slope of the line connecting the CoM to the supporting contact, then a_{com_x} is positive. Contrastingly, if the slope a_i is larger than the slope of the line connecting the CoM and CoP, then a_{com_x} will be negative. This relationship can be represented as the difference between the angles of the CoM path and the CoM-foot line, namely,

$$\alpha_{\text{attack}} = \text{atan}(a_i) - \text{atan}\left(\frac{p_{com_z} - p_{cop_{kz}}}{p_{com_x} - p_{cop_{kx}}}\right). \tag{5.1}$$

For clarity, we will define $\ddot{x} \triangleq a_{com_x}$ and similarly, $\ddot{z} \triangleq a_{com_z}$. We also know that if we are approximating the CoM path with linear piecewise functions, then $\ddot{z} = a_i\, \ddot{x}$, where a_i is the slope of the CoM path at any given time.

First, we will consider the case where a_i is positive but α_{attack} is negative as is depicted in the plot on the right of Figure 5.3. In this situation, $\ddot{x}$ is positive which implies that $\ddot{z}$ is positive as well. This poses an issue since the CoM must have zero velocity in the z-direction at the apex of the jump. If the CoM begins the jump with a positive upward velocity, it must decelerate downwards before it reaches its peak. Therefore, the angle of attack cannot be negative leading up to the peak of the planned trajectory. If we look at the case where a_i is positive and α_{attack} is positive, as is the case in the plot on the left in Figure 5.3, then we will see that $\ddot{x}$ and $\ddot{z}$ will both be negative and there will be the necessary deceleration before the peak that is required to make the vertical velocity zero at that point. From this analysis we have determined that $\ddot{x} < 0$ is an upper bound during the phase before the peak of the CoM path, but it is important to note that there is a lower bound on $\ddot{x}$ as well.

Since the foot is not pinned to the board, the direction in which it can apply a force is limited, i.e., it can only push into the supporting board, not pull away from it. This means that the reaction force applied by the board must be in a direction that lies on the same side of the board as the human. From this understanding, the following analysis can be performed. We know that through balance of forces,

$$\begin{pmatrix} f_{r_x} \\ f_{r_z} \end{pmatrix} = \begin{pmatrix} \ddot{x} \\ \ddot{z} + g \end{pmatrix} M, \tag{5.2}$$

where f_{r_x} and f_{r_z} are the reaction forces in the x-direction and z-direction,

respectively, and M is the total mass of the system. We also know that,

$$\ddot{z} = a_i \, \ddot{x}. \tag{5.3}$$

Substituting Eq. (5.3) into Eq. (5.2) we get,

$$\begin{pmatrix} f_{r_x} \\ f_{r_z} \end{pmatrix} = \begin{pmatrix} \ddot{x} \\ a_i \, \ddot{x} + g \end{pmatrix} M. \tag{5.4}$$

Next, we can say that since the direction of the reaction force must be on the same side of the board as the human,

$$f_{r_N} > 0, \tag{5.5}$$

where f_{r_N} is the force normal to the board. If we assume that γ is the angle of the board measured from the vertical axis, then we can use the rotation matrix,

$$R(\gamma) = \begin{pmatrix} \cos(\gamma) & -\sin(\gamma) \\ \sin(\gamma) & \cos(\gamma) \end{pmatrix}, \tag{5.6}$$

to transform reaction forces from the global frame to the board frame in the following way,

$$\begin{pmatrix} f_{r_N} \\ f_{r_b} \end{pmatrix} = R(\gamma) \begin{pmatrix} f_{r_x} \\ f_{r_z} \end{pmatrix}, \tag{5.7}$$

where f_{r_b} is the reaction force along the board. In this example, we will assume a configuration where the board is rotated counterclockwise from the vertical axis. In the case where the board is rotated clockwise, we would use the rotation matrix,

$$R(\gamma) = \begin{pmatrix} \cos(\gamma) & \sin(\gamma) \\ -\sin(\gamma) & \cos(\gamma) \end{pmatrix}. \tag{5.8}$$

Evaluating Eq. (5.7) for f_{r_N} we get,

$$f_{r_N} = f_{r_x} \cos(\gamma) - f_{r_z} \sin(\gamma), \tag{5.9}$$

and applying Eq. (5.5) gives us,

$$f_{r_x} \cos(\gamma) - f_{r_z} \sin(\gamma) > 0. \tag{5.10}$$

If we then substitute in Eq. (5.4) and divide through by M we get,

$$\ddot{x} \cos(\gamma) - (a_i \ddot{x} + g) \sin(\gamma) > 0. \tag{5.11}$$

Rearranging and solving for $\ddot{x}$ gives,

$$\ddot{x} > \frac{g}{\cot(\gamma) - a_i}. \tag{5.12}$$

Finally, combining this with our initial angle of attack analysis we can say that leading up to the peak of the jump, the acceleration in the x-direction must lie within the region,

$$\frac{g}{\cot(\gamma) - a_i} < \ddot{x} < 0. \tag{5.13}$$

Through this analysis, we can determine the feasibility of certain selected CoM trajectories based on the planned trajectory and the angle, from the vertical, of the supporting board. Figure 5.4 shows three figures with reaction forces in different directions. The middle two figures show reaction forces that satisfy Eq. (5.13) while the figure on the far right shows a reaction force that does not.

Another interesting case comes when the angle of attack is zero, i.e., when the slope of the CoM path a_i matches the slope of the line connecting

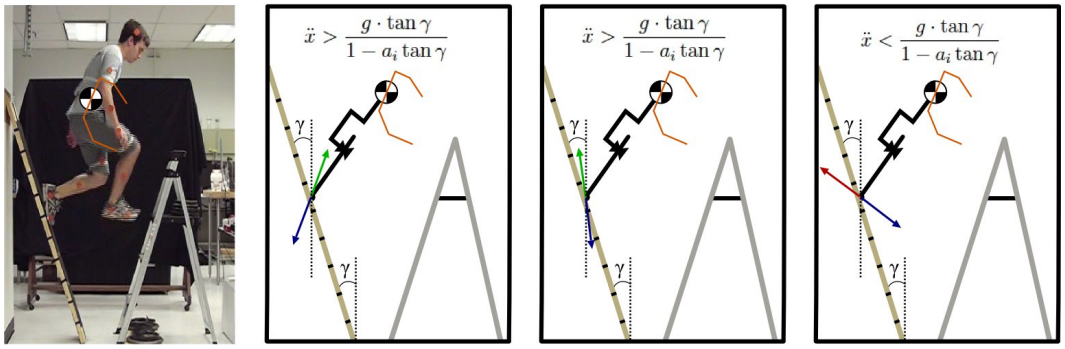

Figure 5.4: **Reaction force limitations during flight phase:** This figure depicts reaction force given possible CoM accelerations in the x-direction. The image on the far left shows the system being modeled and the orange line represents an arbitrary CoM trajectory. The figures in the middle depict potential reaction forces (green arrows) that are within the range of physically feasible values while the image on the far right depicts a potential reaction (red arrow) force that is not feasible.

the CoM and foot. In such a case, $\ddot{x} \to \infty$ as the CoM continues along that trajectory so long as there is an ability to apply a force on the CoM. In reality, at some point the foot would lose contact, once physical joint limits were reached, and leap into the air eliminating the ability for the system to continue to exert a force on the CoM. From this we can infer that it is best to follow a trajectory along the line connecting the contact point and the CoM in order to jump with a maximum velocity.

5.3.2 Analysis of takeoff and landing phases

We now consider further the maneuver of leaping from a given ladder step to a higher one as shown in Figure 5.2. To tackle the dynamics involved in the maneuver and to develop a predictive motion plan for it, we resort to

Algorithm 1 Motion planner for multi-contact jumping (forward) and landing (backward) phases

choose perturbation $\epsilon > 0$ for forward or $\epsilon < 0$ for backward rec.
use Eq. (4.11) to compute Multi-Contact Matrices $C_{k(\forall k)}$
use Eq. (4.13) to compute $C_{fk(\forall k)}$, $C_{tk(\forall k)}$
using Eq. (4.14) to search over feasible $\ddot{x}_{k(\forall k)}$ and $f_{tk(\forall k)}$ values
set $x_{k(k=1)}$ equal to start (forward) or end (backward) point
set $\dot{x}_{k(k=1)} = 0$ and $\dot{z}_{k(k=1)} = 0$ due to boundary conditions
while distance to forward / backward horizon $\neq 0$ **do**
  extract $z_{k+1} = a_i\ x_k + b_i$
  extract $\ddot{z}_{k+1} = \ddot{x}_{k+1}/a_i$
  use Eq. (2.23) to infer $\dot{z}_{k+1}$
  use Eq. (2.24) to infer z_{k+1}
  extract $x_{k+1} = (z_{k+1} - b_i)/a_i$
  extract $\dot{x}_{k+1} = \dot{z}_{k+1}/a_i$
  change piecewise segments $(a_i,\ b_i)$ when appropriate
  use Eq. (4.14) to determine reaction forces f_{rk}
  check that reaction forces f_{rk} are within friction cones
end while

the two powerful methods presented in Chapters 2, 3 and 4, namely numerical recursions and the Multi-Contact Matrix. In this motion sequence, a human subject leaps upward from the second to the third step of a ladder by means of the supporting wall board.

Our approach can be summarized as follows. First, we derive a center of mass geometric path. In this case study, we use a piecewise linear approximation of the CoM path obtained from motion capture of a human but it can be chosen arbitrarily if desired. We then consider three distinctive phases corresponding to a multi-contact takeoff phase, a single-contact flight phase, and a multi-contact landing phase. Based on the designed path, we first solve the

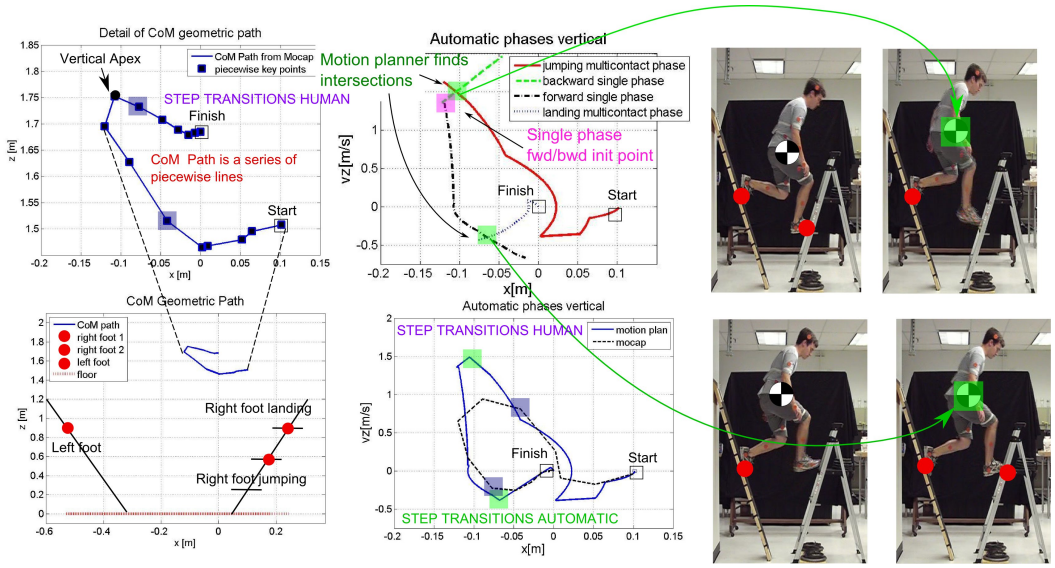

Figure 5.5: **Contact transition planner for gap leaping:** This composed figure depicts details about the planning strategy used to synthesize a leaping maneuver.

single-contact flight phase by means of numerical integration. Next, we solve the takeoff and landing phases by means of the Multi-Contact Matrix and also numerical integration. Finally, we implement a contact transition planner, based on finding intersection points in state-space between multi-contact and single-contact phases.

Before starting to synthesis the motion, let us analyze the behavior shown in Figure 5.2. The subject accelerates his body backward (takeoff phase) to gain momentum to leap upward (flight phase) and land on the next ladder step (landing phase). Motion capture is conducted enabling the extraction of CoM geometric paths and CoM state-space curves as shown in the graphs that accompany the figure. We then approximate the CoM path using linear

piecewise segments. Since we lack force plates on the surfaces in contact, we estimate contact reaction forces by using Algorithm 1. The results of this estimation are shown in the center bottom plot.

We now consider synthesizing an artificially generated maneuver that can leap the steps in a way that is similar to the human. The results of this process are shown in Figure 5.6. For simplicity, we use the discretized version of the CoM geometric path from the human shown on the bottom left graph of Figure 5.2. We divide the synthesis problem into 3 separate parts. First, we use Algorithm 2 to derive flight phase data. This algorithm can be summarized as follows. We choose an initial point on the CoM geometric path perceived as belonging to the single-contact flight phase. We then search over candidate starting vertical velocities and apply numerical integration to derive the natural dynamics of the movement over the geometric path. We validate the initial velocity if its forward projection reaches the vertical apex with zero vertical velocities, meaning that the center of mass can start falling. Because we don't know to what extent the single-contact phase belongs to the different segments of the CoM geometric path, we implement forward and backward recursions over horizons that we believe are beyond the points of liftoff and landing.

We then solve the multi-contact takeoff and landing phases by means of Algorithm 1 which can be summarized as follows. We compute the Multi-Contact Matrix along all data points over the CoM geometric path. We then search over candidate acceleration and tension pairs and apply numerical in-

Algorithm 2 Motion planner for single-contact flight phase (forward/backward strategy)

{forward recursion}
choose perturbation $\epsilon > 0$
set $x_{k(k=1)}$ to be on flight zone
search $\dot{z}_{k(k=1)}$ to reach vertical apex
while distance to forward horizon $\neq 0$ **do**
  extract $z_k = a_i\, x_k + b_i$
  use Eq. (2.20) to determine $\ddot{x}_k$
  extract $\ddot{z}_k = a_i\, \ddot{x}_k$
  use Eq. (2.23) to infer $\dot{z}_{k+1}$
  use Eq. (2.24) to infer z_{k+1}
  extract $x_{k+1} = (z_{k+1} - b_i)/a_i$
  extract $\dot{x}_{k+1} = \dot{z}_{k+1}/a_i$
  change piecewise segments $(a_i,\ b_i)$ when appropriate
  check that $\dot{z}_{k(k=apex)} = 0$
end while
{backward recursion}
choose perturbation $\epsilon < 0$
use $x_{k(k=1)}$ equal to previous initial value
use $\dot{z}_{k(k=1)}$ from previous vertical apex search
while distance to backward horizon $\neq 0$ **do**
  extract $z_k = a_i\, x_k + b_i$
  use Eq. (2.20) to determine $\ddot{x}_k$
  extract $\ddot{z}_k = a_i\, \ddot{x}_k$
  use Eq. (2.23) to infer $\dot{z}_{k+1}$
  use Eq. (2.24) to infer z_{k+1}
  extract $x_{k+1} = (z_{k+1} - b_i)/a_i$
  extract $\dot{x}_{k+1} = \dot{z}_{k+1}/a_i$
  change piecewise segments $(a_i,\ b_i)$ when appropriate
end while

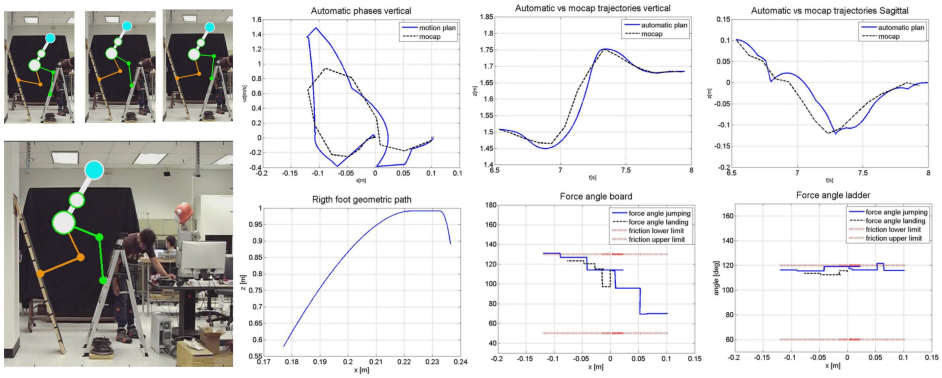

Figure 5.6: **Synthesis results of gap leaping using motion planner:** Shown here is a synthesized leaping motion including an artificially generated CoM behavior based on seeded CoM trajectories and contact plan.

tegration to project the movement over a horizon. The takeoff phase involves a forward projection while the landing phase involves a backward projection which needs to be considered in choosing the perturbation sign. Putting together the previous single and multi-contact recursions lead to the top center graph of Figure 5.5. As we can see, the takeoff and landing phases intersect the flight phase at different points (shown in green on the graph).

Having solved all phases of the movement, we consider finding contact transitions by means of a contact planner. Because we operate in state-space, crossing points between phases imply continuity on position and velocity. As such, the intersections previously discussed are precisely the moments at which contacts need to change to follow the path. For instance, to switch from takeoff to free flight phase, we need to remove the right foot contact at the intersection between the jumping and the backward flight phases. The final motion plan is shown on the bottom center graph of Figure 5.5 against the one extracted

from the human. As we can notice, they are remarkably similar. One of the main differences is that the synthetic path reaches higher velocities during the jumping phase than what the motion capture (mocap) data extraction process shows. However, when synthesizing the movement based on the proposed planner, shown in Figure 5.6, the time trajectories of the vertical and frontal CoM behavior look very similar to the human. Therefore, we believe that the difference in velocities are due to the low sampling rate of the marker data 0.1[s] which means that the peak velocities may have been cut off.

Figure 5.6 depicts the synthetic maneuver based on the planning strategy we have proposed. A time based reconstruction of the vertical and frontal trajectories is also shown against the same data extracted from the human. The trajectories are very similar, demonstrating the validity of the proposed planning methodology. Also, reaction forces of the synthetic maneuver are shown to remain within boundaries of the surfaces in contact. Finally, we show an arbitrary right foot geometric path created with a trajectory generator (not described here) to ascend one step. This foot trajectory was used only for generating the images shown on the left in Figure 5.6 and had no affect on our calculations.

Chapter 6

Conclusion and Future Work

Locomotion and extreme maneuvers in very rough terrain and along near vertical surfaces can be formulated as a non-linear dynamical process, which in general has no closed-form solution. We have resorted to a subset of numerical approximation, namely numerical integration, as an effective tool to predict state-space curves of CoM behavior. By cascading multiple phase curves of CoM behavior around step contacts and finding intersection points, we have generalized the planning of locomotion curves for arbitrary terrains. These prediction and planning methods represent important contributions to the area of motion planning.

The strong correlation of CoM behavior from the motion capture of humans and the automatic planner shown in Chapter 3 demonstrates the validity of our methods. However, to be deployable our method must further include multi-contact stages such as when two feet are in contact with the ground for some period of time. The multi-contact model was introduced in Chapter 4 where we presented the Multi-Contact Matrix as a tool in this modeling process and described its ability to relate CoM behavior and internal tension forces to reaction forces at points of contacts.

Combining the multi-contact methods used to calculate reaction forces with the single contact methods used to find step transitions, we were able to predict CoM behavior and contact transition for a leaping maneuver consisting of both multi-contact and single contact phases as shown in Chapter 5. This is an important step towards motion planning for realistic locomotion in which there are periods of dual contact and also for extreme maneuvers which almost always require periods with at least two points of contact.

The methods presented in this paper provide the framework for extensive optimization possibilities. As we have shown, our planning algorithms are robust to any set of input parameters that will fulfill physical constraints. This creates an immense space of possible motion plans all, of which are feasible, but potentially few of which are optimal for certain performance specifications such as minimizing cost of transport or time of traversal. Optimal trajectories could be generated through an iterative search-based technique, but there is an opportunity for implementing more advanced optimization methods as well.

Another area of future research relates to the expansion of these prediction methods to three-dimensional environments. This involves reducing equations of motion in the lateral y-direction in similar ways to what we have done in the plane consisting of the vertical z-direction and frontal x-direction and using numerical integration to approximate CoM behavior and find step transition points. This includes seeding two-dimensional planes on which the CoM can exist rather than simply a one-dimensional path. A search-based method can then be used to find lateral foot location that generates the same

step transition times as the frontal-vertical plane analysis. Research in this area is currently being explored by members of the HCR Laboratory at UT-Austin.

As stated, in the introduction the HCR Laboratory, Dr. Sentis and I aim to develop methods that can be used in the design of robots and assistive devices with similar capabilities as humans. This includes implementation in physical systems to validate the algorithms we create beyond what simulations can provide. In the Fall of 2011, the HCR Laboratory teamed with Meka Robotics to develop a state of the art bipedal robot, HUME, designed with the physical capability to perform the extreme maneuvers presented in the earlier chapters. As of the writing of this thesis, HUME has been in the HCR Laboratory for one month and is currently in the early stages of control and performance testing. One of the objectives of the researchers working on this project is to implement motion planning algorithms on HUME in an effort to execute parkour and freerunning type maneuvers. This will be done in coordination with the Whole-Body-Control framework developed in [18] and is currently being implemented in the Dreamer robot at the HCR Laboratory.

Appendices

Appendix A

Effect of Moments During Locomotion

In this appendix, we briefly explain why we we assume a point mass, and therefore, no moments about the CoM during the analysis of the experiments in the body of this thesis. The moment about the CoM of a planar system comprised of many rigid bodies can be describe as,

$$M_{com} = \sum_{i=1}^{n} J_i \, \ddot{\theta}_i \tag{A.1}$$

where M_{com} is the moment about the systems CoM at each time-step, J_i is the rotational inertia of each link about that body segment's CoM, $\ddot{\theta}_i$ is the angular acceleration of each link about its CoM in the global frame at each time-step and n is the number of body segments.

Let us apply this definition to the validation experiment presented in Chapter 3. By tracking the locations of each joint as well as the location of each body segment CoM, via motion capture, we can calculate the orientation of each body segment in the global frame and each time-step and then differentiate to find angular accelerations. Using information on the rotational inertia of body segments described in [27] and the angular accelerations, we can use Eq. (A.1) to calculate the moments about the CoM in the y-direction (orthogonal to the plan of motion) at each time-step. As we can see in the

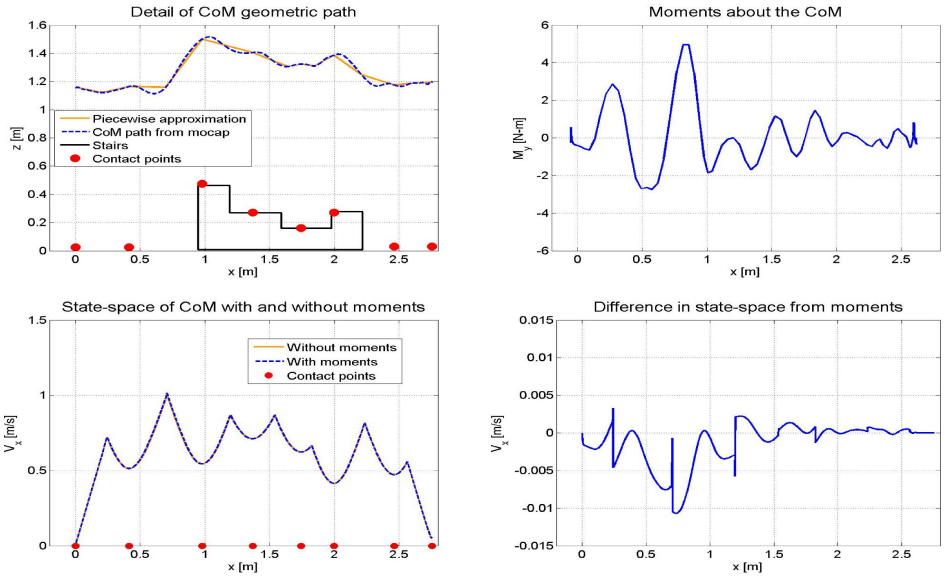

Figure A.1: **Effects of moments on locomotion:** This figure shows the effect moments had in the locomotion experiment described in Chapter 3. The upper left plot shows the geometric path followed by the CoM. The lower left plot shows automatically generated state-space behavior with moments and without the inclusion of moments. The upper right plot shows the moments about the CoM and the lower right plot shows the difference in velocities generated though the motion planner with and without the inclusion of moments.

upper right plot of Fig A.1, the moments about the CoM are small during the locomotion sequence being examined. This is due to the lack of excess motion by the torso and arms during the maneuver and the canceling effect the legs have on one another since they rotate in opposite directions during each step. The two bottom plots in Fig A.1 show how little an effect the moments have on the automatic motion plan. The figure on the left shows that the plots of the state-space behavior of the CoM with or without the inclusion of moments are nearly indistinguishable and the figure to its right shows why. We can see

there that the difference in velocities at any give time-step is only about 1% of the actual velocity with a maximum difference of only about 0.01[m/s].

Another reason to assume there are no moments about the CoM is due to the fact that it is nearly impossible to know what the moments will be when planning an arbitrary motion. Moments are a function of angular acceleration which is a function of the rate at which the configuration of the system is changing at each time-step. However, without an understanding of the way the system's CoM will behave or where step transitions should be made (i.e., a motion plan) there is no way to accurately plan feet trajectories. Without feet trajectories, system geometric configurations at each time-step cannot be found, meaning moments about the CoM cannot be found. This leads to a circular problem, the need for information about moments before an accurate motion plan can be produced contrasted with the need for a motion plan before moments can be found. One way to deal with this issue is to assume one point mass for the system and ignore moments since, as shown in Fig A.1, in some cases they have a negligible effect. Another option is to use a recursion method.

The recursion method consists of first running the motion planning algorithm (including terms involving moments) with arbitrarily chosen values for the moments at each time-step. Using this CoM behavior, feet trajectories can be generated leading to body segment orientation and, finally, body segment angular accelerations. With an understanding of the inertias of each link in the system, moments about the CoM can be calculated. These moment

values can be fed back into the motion planning algorithms to generate a new CoM behavior sequence. Moments can be calculated from this motion plan and fed back into the planner again and so on. Eventually the CoM behavior and the moments about the CoM will converge such that the moments plugged into the motion planning algorithm are the same as the ones calculated from resulting system dynamics.

Appendix B

Single Contact Brachiation

This appendix contains a brief description of research we performed on the effect of moments about the CoM on motion planning during brachiation. Brachiation is a form of arboreal locomotion usually associated with primates in which the subject traverses space by swinging with only the arms. In the sport of rock climbing this type of maneuver is commonly called campusing. The body of this thesis ignores moments about the CoM for reasons described in Appendix A. Through analysis of rock climbers performing brachiation, we have determined that moments have a much larger and very relevant role in CoM behavior during these maneuvers and they should not be ignored.

First, let us consider the difference between the model used for locomotion and the model needing to be used for brachiation. For locomotion, we use inverted pendulum dynamics to find accelerations of the CoM in the x-direction as a function of some known parameters (see Eq. (2.20)). In the case of brachiation, we must use a traditional pendulum model but can use the same general function given by Eq. (2.20) to find acceleration in the x-direction. We know this because Eqs. (2.1) and (2.3) pertaining to the balance of moments and balance of forces, respectively, are the same for both models.

Figure B.1: **Single contact brachiation maneuver sequence:** Here we see a subject campusing along a rock ledge. The orange line depicts the trajectory of the climbers CoM as he traverses from his right to left.

This allows us to implement the same motion planning algorithm used in the body of this thesis to calculate CoM behavior during brachiation.

Let us consider the motion of a climber campusing across a ledge as depicted in Figure B.1. We used the motion capture and video processing techniques described in Section 3.2.1 to extract trajectories of the CoM of each body segment as well as the CoM of the entire system. Joint trajectories as well as contact points were also tracked. A linear piecewise approximation of the CoM path was seeded into the motion planning algorithm (see upper left of Figure B.2) along with boundary condition values also taken from the human. These boundary conditions did not generate a feasible motion plan. The velocities used at the apex of each swing (the instant when the CoM was directly below the point of contact) were too small to allow the CoM to travel far enough in the x-direction to reach the switching point. Graphically, this presents itself as a discontinuity in the state-space plot, i.e., no intersection between forward and backward propagations of neighboring steps. This was

cause for concern as this problem contradicts our prediction that the state-space profiles from the automatic planner should match the data collected during motion capture if the same path and boundary conditions are used.

In an attempt to understand the issue more fully, seeded boundary conditions were adjusted away from the values obtained from the human. By increasing the magnitude of the apex velocities, a state-space solution for the entire climbing sequence was able to be generated. This solution, which used apex velocities that gave continuous trajectory, is depicted as the green line in the lower left of Figure B.2. We see, though, that as expected, the state-space profile generated using the larger velocities deviates from the human state-space behavior more than can be dismissed as experimental error.

In trying to understand the results of this trial, we began to consider the effect moments might play. We knew, as described in Appendix A, moments about the CoM had a negligible effect on motion planning in our first studies, but noticed there was much more rotation of the body segments while swinging than there was between steps during locomotion. This substantial rotation, especially of the body segments with large inertias such as the torso and legs, hinted at the potential for large moments that could have an effect on CoM behavior. Using the same method described in Appendix A, angular accelerations and moments of inertia of the body segments for each body segment were calculated and used to find the total moments about the system CoM at each time-step. The profile of moments orthogonal to the plane of motion are shown in the upper right plot in Figure B.2. In the sequence

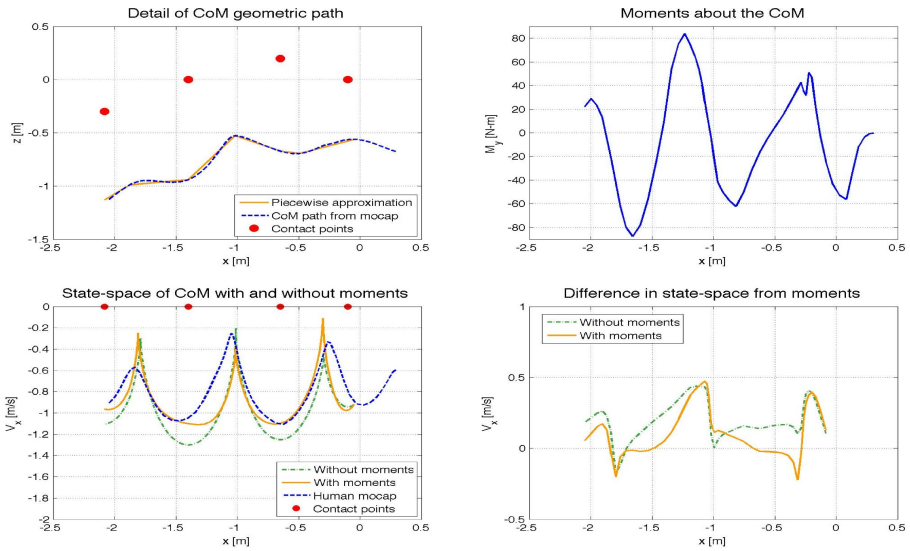

Figure B.2: **Effects of moments on brachiation:** This figure shows the effect moments had in a brachiation sequence shown in the previous figure. The upper left plot shows the geometric path followed by the CoM. The lower left plot shows automatically generated state-space behavior with moments and without the inclusion of moments as well as the behavior of the human generated from motion capture data. The upper right plot shows the moments about the CoM and the lower right plot shows the difference in velocities generated thought the motion planner with and without the inclusion of moments.

being studied, the moments approach a maximum magnitude of 90[N-m] as opposed to 3[N-m] as was the case during the locomotion sequence examined in Chapter 3. When these moments were included in the motion planning algorithm and the original boundary conditions taken from the human were used as seeded parameters, a continuous state-space profile was generated. This profile is depicted as the orange line in the lower left of Figure B.2. We can clearly see that the state-space portrait generated when moments about the CoM were included matches that of the human much more closely than

the one generated without moments and with adjusted apex velocities. The lower left plot of Figure B.2 depicts the difference in velocities between the behavior generated with and without the inclusion of moments.

From this study, we can conclude that moments can have a substantial effect on CoM behavior during certain motion sequences. However, these sequences must include high angular acceleration of body segments with large inertias such as is the case in some instances of brachiation.

Appendix C

Multi-Contact Brachiation

This appendix extends the work covered in Appendix B on motion planning during brachiation and begins to examine the dynamics of multi-contact states during these maneuvers with the specific goal of examining the role of moments. Similar to the motion planning study, we began with video of a subject swinging from both hands. A sequence of frames from this video is shown in Figure C.1. The video was processed using the methods described in Section 3.2.1 to extract the subject's CoM behavior as well as the behavior of his joints and the CoM of his body segments.

Similar to Appendix B, this data was used to calculate moments about the subject's CoM via Eq. (A.1). Once these system kinematics and dynamics were known, we were able to begin to predict the reaction forces at the hands through the use of the Multi-Contact Matrix described in Chapter 4. While this study was similar to the one conducted in Section 5.2, there were two significant differences. First, the frictional contact constraints of climbing holds are much more difficult to model than the foot contacts of the first study and second, the effects of moments were not examined in that study.

The contact constraints on the hands during climbing are more similar

Figure C.1: **Multi-contact brachiation maneuver sequence:** Here we see a subject swinging from his left two right while supported between two contact points, one at each hand. The orange line depicts the path of the CoM during the climbing sequence.

to a joint that is pinned to the ground rather than a contact that is resting on the ground. For this reason, a friction cone is no longer a valid model for analyzing feasible reaction forces. We can instead imagine a friction sphere, or possibly an asymmetric shape, as the model needing to be used. Also, in the case where the hand is the supporting contact, the magnitude of possible reaction forces is not only a function of friction properties but also a function of finger strength. These properties may not be the same for all directions based on the hand hold, resulting in an asymmetric contact constraint shape. At the time of analysis, information regarding hand strength and friction properties between the skin and rock holds was unknown so the friction shapes were not able to be examined. This is a potential area for future research.

Two separate comparison studies were performed on reaction force. The first study compared the reaction forces with and without the inclusion

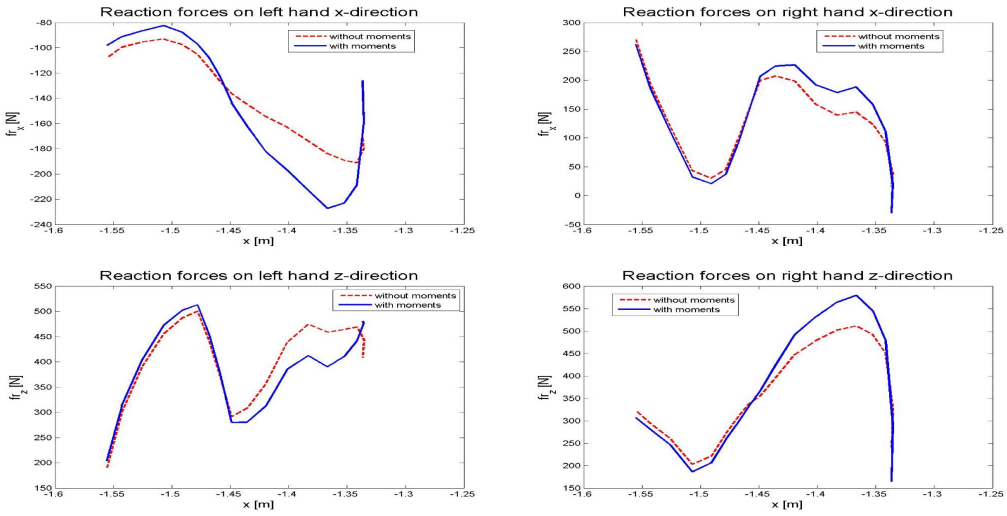

Figure C.2: **Reaction forces with and without moments:** This figure depicts the reaction forces at the hands during the swinging motion shown in Figure C.1. The red line represents the forces without the inclusion of moment while the blue line does include moments. In both cases a constant nominal tension force of -250[N-m] was assumed to be acting between the hands.

of moments about the CoM while maintaining a constant nominal internal tension force between the hands. The second study compared the reaction forces at the hands when different tension forces were applied. In the second study, moments about the CoM were included in calculation and the different tension forces used remained constant over the entirety of the motion sequence.

Let us look at the results of the first study. For these trials, a constant nominal tension force of -250[N-m] was assumed when moments about the CoM were and were not included in calculations. The tension force chosen was negative to indicate the hands are applying forces towards each other, as one would assume is the case when climbing, rather than away from each

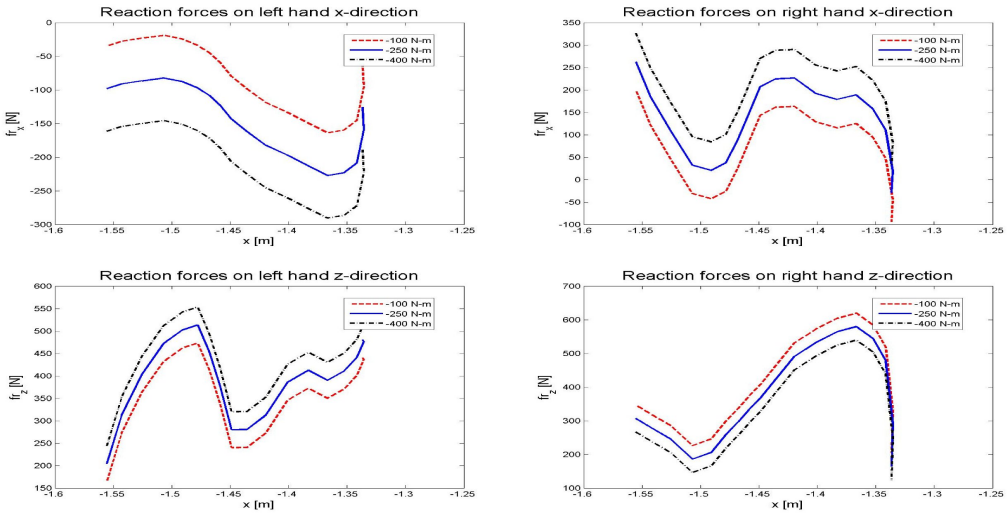

Figure C.3: **Reaction forces with various moments:** This figure shows the reaction forces at the hands during the swinging motion shown in Figure C.1 but with varying tension forces. The black, blue and red lines depict the reaction forces when -100[N-m], -250[N-m] and -400[N-m] are applied, respectively. In all cases the tension force was held constant over the entire swinging sequence.

other. The magnitude was chosen arbitrarily, loosely based on the projection of reaction forces onto the vector connecting the hands of a passive static system with similar geometry and mass properties. Figure C.2 shows the results of both trials. It is clear that the inclusion of moments about the CoM causes a significant difference in reaction forces at each hand in both the x-direction and the z-direction. In an attempt to validate our results, we calculated the sum of the integrals of all the reaction forces with respect to the x-direction in each trial to find the total external work done by the system over the course of the motion. As expected, these values were the same since including internally generated moments should not affect external work. This result lends validity

to our reaction force calculation methods.

Now, let us look at the results of the second study. In this case, we used the same motion parameters as in the first trial with the inclusion of moments but applied various tension forces to the system. Three different tension forces held constant over the course of the each trial were used. They were -100[N-m], -250[N-m] and -400[N-m]. These values were chosen arbitrarily around the tension used in the first study but kept negative to comply with our assumption that the tension forces at each contact point toward one another. The results of these trials are shown in Figure C.3. The shapes of the plots for each trial are similar but the magnitude of the reaction forces increase as one might expect. The plot in the upper right of the figure (reaction forces of the right hand in the x-direction) is of particular interest. We can see that when a tension force of -100[N-m] is applied, the reaction force in the x-direction becomes negative for a period during the course of the motion. Without a further understanding of the contact constraints described earlier, it is not possible to know whether this exceeds those limits, however, a intuitive understanding of human physiology might imply that applying a force away from the CoM while having a hook-like grasp on a hold would be difficult. This is a speculative assumption that would require further examination to verify and would be an potential area for biomechanical analysis to be incorporated.

Based on the results of these studies, we can decisively conclude that moments about the CoM play a significant role in the reaction forces applied at the points of contact during multi-contact phases of brachiation. This effect

could define tension force profiles that satisfy contact constraints yet would not be feasible if moments were ignored. Conversely, certain tension profiles that are feasible without the inclusion of moment may be infeasible when moments are accounted for.

Bibliography

[1] K. Bouyarmane and A. Kheddar. Multi-contact stances planning for multiple agents. In *Proceedings of the IEEE International Conference on Robotics and Automation*, Shanghai, May 2011.

[2] T. Bretl and S. Lall. Testing static equilibrium for legged robots. *IEEE Transactions on Robotics*, 24(4):794–807, August 2008.

[3] Katie Byl and Russ Tedrake. Metastable walking machines. *The International Journal of Robotics Research*, 28(8):1040–1064, 2009.

[4] C. Collette, A. Micaelli, C. Andriot, and P. Lemerle. Robust balance optimization control of humanoid robots with multiple non coplanar grasps and frictional contacts. In *Proceedings of the IEEE International Conference on Robotics and Automation*, Pasadena, USA, May 2008.

[5] A. Goswami, B. Espiau, and A. Kermane. Limit cycles and their stability in a passive bipedal gait. In *Proceedings of the IEEE International Conference on Robotics and Automation*, pages 246–251, April 1996.

[6] K. Harada, S. Kajita, K. Kaneko, and H. Hirukawa. Zmp analysis for arm/leg coordination. In *Proceedings of the IEEE/RSJ International Conference on Intelligent Robots and Systems*, pages 75–81, Las Vegas, USA, October 2003.

[7] K. Hauser, T. Bretl, K. Harada, and J.C. Latombe. Using motion primitives in probabilistic sample-based planning for humanoid robots. In *Workshop on Algorithmic Foundations of Robotic (WAFR)*, New York, USA, July 2006.

[8] S-H. Hyon, J. Hale, and G. Cheng. Full-body compliant humanhumanoid interaction: Balancing in the presence of unknown external forces. *IEEE Transactions on Robotics*, 23(5):884–898, October 2007.

[9] S. Kajita, M. Morisawa, K. Harada, K. Kaneko, F. Kanehiro, K. Fujiwara, and H. Hirukawa. Biped walking pattern generator allowing auxiliary zmp control. In *Intelligent Robots and Systems, 2006 IEEE/RSJ International Conference on*, pages 2993–2999, october 2006.

[10] Ian R Manchester, Uwe Mettin, Fumiya Iida, and Russ Tedrake. Stable dynamic walking over uneven terrain. *The International Journal of Robotics Research*, 30(3):265–279, 2011.

[11] T. McGeer. Passive dynamic walking. *The International Journal of Robotics Research*, 9(2):62–68, 1990.

[12] K.D. Mombaur, H.G. Bock, J.P. Schloder, and R.W. Longman. Self-stabilizing somersaults. *Robotics, IEEE Transactions on*, 21(6):1148 – 1157, december 2005.

[13] Y. Nakamura, H. Hanafusa, and T. Yoshikawa. Mechanics of coordinative manipulation by multiple robotic mechanisms. In *Proceedings of the*

IEEE International Conference on Robotics and Automation, pages 991–998, April 1987.

[14] J.E. Pratt and R. Tedrake. Velocity-based stability margins for fast bipedal walking. In Moritz Diehl and Katja Mombaur, editors, *Fast Motions in Biomechanics and Robotics*, volume 340, pages 299–324. 2006.

[15] M.H. Raibert. *Legged Robots that Balance*. MIT Press, Cambridge, Ma., 1986.

[16] A. Ruina, J.E. Bertram, and M. Srinivasan. A collisional model of the energetic cost of support work qualitatively explains leg sequencing in walking and galloping, pseudo-elastic leg behavior in running and the walk-to-run transition. *Journal of Theoretical Biology*, (237):170–192, 2005.

[17] J Rummel, Y Blum, and A Seyfarth. Robust and efficient walking with spring-like legs. *Bioinspiration & Biomimetics*, 5(4):046004, 2010.

[18] L. Sentis and O. Adviser-Khatib. *Synthesis and control of whole-body behaviors in humanoid systems*. Stanford University, 2007.

[19] L. Sentis and B. Fernandez. Com state space cascading manifolds for planning dynamic locomotion in very rough terrain. In *Proceedings of Dynamic Walking 2011*, Jena, Germany, July 2011.

[20] L. Sentis, J. Park, and O. Khatib. Compliant control of multi-contact and center of mass behaviors in humanoid robots. *IEEE Transactions on Robotics*, 26(3):483–501, June 2010.

[21] M.W. Spong, J.K. Holm, and Dongjun Lee. Passivity-based control of bipedal locomotion. *Robotics Automation Magazine, IEEE*, 14(2):30 –40, june 2007.

[22] B. Stephens and C. Atkeson. Modeling and control of periodic humanoid balance using the linear biped model. In *Humanoid Robots, 2009. Humanoids 2009. 9th IEEE-RAS International Conference on*, pages 379 –384, december 2009.

[23] Takashi Takuma and Koh Hosoda. Controlling the walking period of a pneumatic muscle walker. *The International Journal of Robotics Research*, 25(9):861–866, 2006.

[24] E.R. Westervelt, J.W. Grizzle, C. Chevallereau, J.H. Choi, and B. Morris. *Feebdack control of dynamic bipedal robt locomotion.* CRC Oress, 2007.

[25] D. Williams and O. Khatib. The virtual linkage: A model for internal forces in multi-grasp manipulation. In *Proceedings of the IEEE International Conference on Robotics and Automation*, pages 1025–1030, Atlanta, USA, October 1993.

[26] M. Wisse, A.L. Schwab, R.Q. van der Linde, and F.C.T. van der Helm. How to keep from falling forward: elementary swing leg action for passive

dynamic walkers. *Robotics, IEEE Transactions on*, 21(3):393 – 401, june 2005.

[27] F.E. Zajac and J.M. Winters. Modeling musculoskeletal movement systems: joint and body segmental dynamics, musculoskeletal actuation, and neuromuscular control. *Multiple muscle systems: Biomechanics and movement organization*, pages 121–148, 1990.

[28] M. Zucker, J.A. Bagnell, C.G. Atkeson, and J. Kuffner. An optimization approach to rough terrain locomotion. In *Robotics and Automation (ICRA), 2010 IEEE International Conference on*, pages 3589 –3595, may 2010.